FEDERAL UNIVERSITY OF ITAJUBÁ - UNIFEI
GRADUATE PROGRAM IN ELECTRICAL ENGINEERING

Dynamic Machine Model in Complex Plane

Francisco Costa Santos

Itajubá, 12 of june of 2024

FEDERAL UNIVERSITY OF ITAJUBÁ - UNIFEI
GRADUATE PROGRAM IN ELECTRICAL ENGINEERING

Francisco Costa Santos

Dynamic Machine Model in Complex Plane

Dissertation submitted to the Graduate Program in Electrical Engineering as part of the requirements to obtain the title of Master of Science in Electrical Engineering.

Concentration Area: Methods for Analysis, Planning and Operation of Electrical Systems

Supervisor: Prof. DSc. Robson Celso Pires
Co-supervisor: Prof. DSc. Zulmar Soares Machado Junior

12 of june of 2024
Itajubá

FEDERAL UNIVERSITY OF ITAJUBÁ - UNIFEI
GRADUATE PROGRAM IN ELECTRICAL ENGINEERING

Dynamic Machine Model in Complex Plane

Francisco Costa Santos

Dissertation approved by the examining board in 11 of July of 2024, giving the author the title of **Master of Science in Electrical Engineering.**

Examination Board:
Prof. Dr. Robson Celso Pires
Prof. Dr. Zulmar Soares Machado Junior
Prof. Dr. Benedito Isaías Lima Fuly
Dr. Jorge Luiz de Araujo Jardim (HPPA)

Itajubá
2024

Francisco Costa Santos
Dynamic Machine Model in Complex Plane - / Francisco Costa Santos. – Itajubá, 17 de julho de 2024-
78 p. : il. (algumas color.) ; 30 cm.

Supervisor: Prof. Dr. Robson Celso Pires

Dissertation (Master's Degree)
Federal University of Itajubá - UNIFEI
Graduate Program in Electrical Engineering, 12 of july of 2024.

1. Dynamic Measurements. 2. Machine Classical Model in Complex Plane Using Simulink. I. Supervisor Dr. Robson Pires. II. Federal University of Itajubá.

CDU 07:181:009.3

Francisco Costa Santos

Dynamic Machine Model in Complex Plane

Dissertation submitted to the Graduate Program in Electrical Engineering as part of the requirements to obtain the title of Master of Science in Electrical Engineering.

Dissertation approved. Itajubá, 11 of July of 2024:

Prof. Dr. Robson Celso Pires
Supervisor

Prof. DSc. Zulmar Soares Machado Junior
Co-supervisor

Prof. Dr. Benedito Isaías Lima Fuly

Dr. Jorge Luiz de Araujo Jardim (HPPA)

Itajubá
12 of july of 2024

Acknowledgments

Thanks God, firstly, that gave me strength to accomplish this stage in my life.

To the professor Robson Celso Pires for the knowledgement, patience and dedication during the orientation of this project.

To the professor Doctor Zulmar Soares Machado Junior for the opportunity and support during all the process of building this master's degree thesis.

To FAPEMIG (Fundação de Amparo à Pesquisa do Estado de Minas Gerais) for the finantial support that allowed me to dedicate on full time.

To UNIFEI for supplying all the infrastructure and the technical knowlegment of my masters' degree, which were essentials for the accomplishment of this work.

To my friend, Eduardo Resende, and other friends that directly or indirectly participated of my undergraduate, my eternal thanks.

I would like to thank and dedicate this academic work, also, to the following people: my family, my daughter Isabella, my grandmother Ana Emidia, my mother Ana Lucia, my twin sister Ana Carolina and to all my family.

"The work is not to see so many things that anyone has seen, but thinking what no one yet thought about things that everybody see.
(Arthur Schopenhauer)

Summary

This work presents the implementation of a dynamic classical model of machines on complex domains. For it, it will be considered the state equations of δ and ω. On this way, the algorithm is derived on complex plane. Besides it, this work compares the performance using this classical model on complex plane with the same model formulated in real domain. The test systems evaluated are the IEEE-14 and IEEE-39 bus. And it will be used to validate both results on real and complex planes, a brazilian very known power system program called ORGANON. The analysis of the obtained results, in SIMULINK, demonstrate the computational advantage of the model in complex plane. Such advantage increase as the size of the system gets higher.

Key-words: Dynamic classical model of machines on complex domains. Comparison of the performance.

Abstract

The present work implements a dynamic classical model of machines on complex plane. For this goal, the state equations for the machine angle, δ and for the machine rotor speed, ω, will be developed in complex domain. Moreover, the performance of the classical model of machines on complex plane are compared with its counterpart formulated in the real domain. The proposal is evaluated by using the well known test systems IEEE-9 bus and IEEE-39 bus. Additionally, a brazilian well used dynamics power system program named ORGANON is taken as benchmark for the studied cases. The analysis of the obtained results through the SIMULINK allow to demonstrate the computational advantage of the model in complex plane as the size of the system becomes larger.

Key-words: Dynamic classical model of machines on complex domains. Comparison of the performance.

List of Figures

List of Tables

List of abbreviations and acronyms

CPU	*Central Process Unit*
HPPA	*High Performance Power System Applications*
IEEE	*Institute of Electrical and Electronics Engineers*
INTEL	*Integrated Electronics*
MATLAB	*Matrix Laboratory*
ODE	*Ordinary Differential Equation*
ONS	*National System Operator*
P&D	*Researches and Developments*
RAM	*Random Access Memory*
RK	*Runge-Kutta*
SIMULINK	*Block Diagram Simulation Environment*
SIN	National Interconnected System

List of symbols

A_i	Classical machine model constant i
D	Damping factor
H	The inertia constant
KM	Mutual inductance
L	Own inductance
$L^{''}$	Sub-transient inductance
$L^{'}$	Transient inductance
M	Mutual inductance
P	Park's transformation matrix
P_e	The real power output
S_e	Apparent power
T_M	The mechanical power input conjugate
X	Reactance
$X^{'}$	Transient reactance
$\Delta\omega$	Rotor speed deviation
α	State variable in complex domain
δ	Actual rotor angle in radians
λ	Linkage flux
$(\ \cdot\ )^*$	Denotes the complex conjugate
$(\ \cdot\ )^T$	Denotes the transposed
ω	Actual rotor speed in radians/s
ω_s	Synchronous rotor speed in radians/s
$\overline{E}$	Voltage phasor
$\overline{I}$	Current phasor
$\overline{Y}^{red}$	Reduced Kron admttance matrix of the systems
ϕ	Flux density
$\tau_u^{"}$	Sub-transient constant
θ	Angle between phase A and d axis
i_f	Field current

Contents

1 Introduction

1.1 Initial Considerations

The technological advancements of humanity need, continuously, increases in electrical energy demand [5]. Therefore, the speed of power system to restore its steady state, when submitted to events, is so important to the reliability [6]. Especially, in countries that supply and requires much hidrohidreletric energy, such as Brazil, United States and other countries [7].

The study of the characteristic of an electrical systems, when is submitted to electrical disturbances, is recognized as the study of dynamic of the electric system [8].

The eletromechanical oscilations are related with the oscillations of the rotor angles of the generation machines [9]. Those oscillations happen on many interconnect systems, where the power transmission are through long lines. These oscillations are included on machine models. There are plenty of researches using the electric machine models. Some of them varying the machines parameters or estimating systems voltage and angles. For instances, on [10], the machine parameters can vary when considering the field reconstruction method; On [11], the machine classical model is used to estimate the voltate and angle on bus of electric power systems. In this master's degree will be used the classical model of synchronous machines.

According to [8, 12], the classical model is a model that considers constant the $E_q^{'}$ along the study time. This model considerate some simplifitions of the machines. This representation is used to model far away machines from the principal area, not considering the excitation systems and voltages regulators [1, 8, 13].

One of the common techniques to solve the dynamic ODEs of classical models on simulations of power system behaviors is the fixed step four order RK method. But it's important to use this numerical integration with mathematical cares about the integration step in the context of power system analysis [14, 15].Another types of methods are the variable steps integration ones that utilize trapezoids and Runge-Kutta, as examples, Dormand-Prince and Trapezoidal methods, respectively [16].

The idea of writing the classical model in complex plane, depending on the complex state variable and its complex conjugate, is becoming the equations multi differentiable, because it is going to respect the Cauchy–Riemann criterion [17] and that's the criterion of functions diferenciability. Then, these functions can be linearized, expanded in Taylor series and used in Wirtinger Calculous [18]. These are the advantages of mathematically writing this model in complex plane and, nowadays, it favors the hybrid electric power

systems [19].

The engineering and the applied science are areas that have huge dependency of signals analysis and complex variables to model real variables or at least simulating real physical phenomena. In this way, modeling with numbers in complex domain have its computational and mathematical own characteristics [20]. Considering these characteristics and the recent changes on brazilian power system to hybrid, i.e. including renewable resources, the studies of stability are extremely important [21].

Therefore, the main contribution of this work is presenting the equations of the classical dynamic model in the complex domain using two power systems, showing, yet, a comparative between the same modeling on real and complex domains. For this purpose, two test systens will be used, the IEEE 9-Bus and 39-Bus systems. The computational efficiency of this model shows superior related to the same one formulated on real domain. As contribution of this work, present a efficient algorithm to represent the power systems considering the classical machine model with implementation on MATLAB and SIMULINK.

1.2 Work Organization

In Chapter 2 presents the machine classical model. Furthermore, this chapter shows the fundamentals of the stability conditions of the control system. In Chapter 3, the numerical results of the model using simulink for a 9-bus system and later for the IEEE-39 test system are presented. Finally, Chapter 4 expresses the most relevant conclusions of the work.

2 Theoretical Review

2.1 Synchronous Machine Modeling

2.1.1 Introduction

Considering the Figure 1,

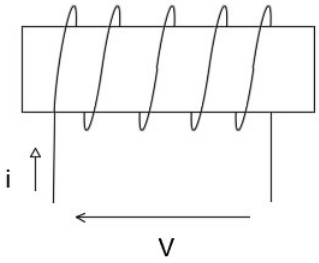

Figure 1 – Basic Electric Machine

By Ohn and Faraday's Laws knowing that the electric voltage for the basic electric machine is represented as (2.1) [1]:

$$v = R\ i + \frac{d(L\ i)}{dt}, \tag{2.1}$$

Where R and L are the electrical resistance and inductance, respectively; i is the current; v is the voltage.

With the saturation absence (2.2):

$$v = R\ i + L\ \frac{d(i)}{dt}, \tag{2.2}$$

Therefore, the instantaneous power is (2.3):

$$v\ i = R\ i^2 + L\ i\ \frac{d(i)}{dt}, \tag{2.3}$$

As (2.4),

$$\frac{d}{dt}\left(\frac{1}{2}\ L\ i^2\right) = L\ i\ \frac{di}{dt}, \tag{2.4}$$

Taking into account a magnet approching to the spiral in (2.5):

$$v = R\ i + L\ \frac{di}{dt} + i\ \frac{d(L)}{dt}, \tag{2.5}$$

Manipulating the previous equation, results (2.6):

$$v\ i = R\ i^2 + \frac{d}{dt}\left(\frac{1}{2}\ L\ i^2\right) + \frac{1}{2}\ i^2\ \frac{d(L)}{dt}, \tag{2.6}$$

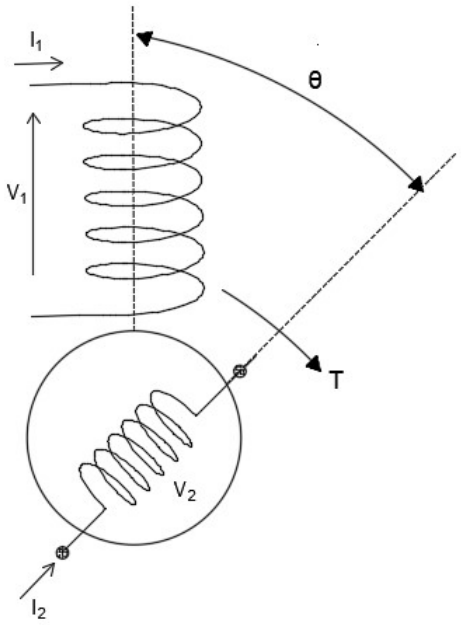

Figure 2 – Basic Machine of Two Windings

Taking into consideration a basic two windings machine, from Figure 2, considering the mutual inductance equal for the two windings, i.e, $M_{12} = M_{21} = M$. Thus, the power equation results (2.8) [1, 2, 22]:

$$\begin{aligned} v_1\ i_1 + v_2\ i_2 = \underbrace{R_1\ i_1^2 + R_2\ i_2^2}_{DissipatedPower} + \underbrace{\frac{d}{dt}\left(\frac{1}{2}\ L_1\ i_1^2 + \frac{1}{2}\ L_2\ i_2^2 + M\ i_1\ i_2\right)}_{MagneticPower} \\ \underbrace{+\frac{1}{2}\ i_1^2\ \frac{dL_1}{dt} + \frac{1}{2}\ i_2^2\ \frac{dL_2}{dt} + i_1\ i_2 \frac{dM}{dt}}_{MechanicPower}, \end{aligned} \tag{2.7}$$

Where R_1 and L_1 are the electrical resistance and inductance for the first winding, respectively; i_1 is the current for the first winding; v_1 is the voltage for winding 1; R_2 and

L_2 are the electrical resistance and inductance for the second winding, respectively; i_2 is the current for the second winding; v_2 is the voltage for winding 2.

And for the electromagnetic conjugate in (2.9):

$$T\,\frac{d\theta}{dt} = \frac{1}{2}\,i_1^2\,\frac{L_1}{d\theta}\,\frac{d\theta}{dt} + \frac{1}{2}\,i_2^2\,\frac{L_2}{d\theta}\,\frac{d\theta}{dt} + i_1\,i_2\,\frac{dM}{d\theta}\,\frac{d\theta}{dt}, \tag{2.8}$$

$$\underbrace{T}_{T_{em}} = \frac{1}{2}\,i_1^2\,\frac{dL_1}{d\theta} + \frac{1}{2}\,i_2^2\,\frac{dL_2}{d\theta} + i_1\,i_2\,\frac{dM}{d\theta}, \tag{2.9}$$

Where T is the electromagnetic conjugate and θ is the rotor angle.

2.1.2 Linkage Flux Equations - Phase Coordinates

The machine is called synchronous when the speed of the magnetic field is the same of rotor speed. All synchronous machine have two parts: the rotor and the stator. Its stators have thin blades, which the linkage magnetic flux across, reducing the loss, for instance, as seen on Figure 3 [1, 23].

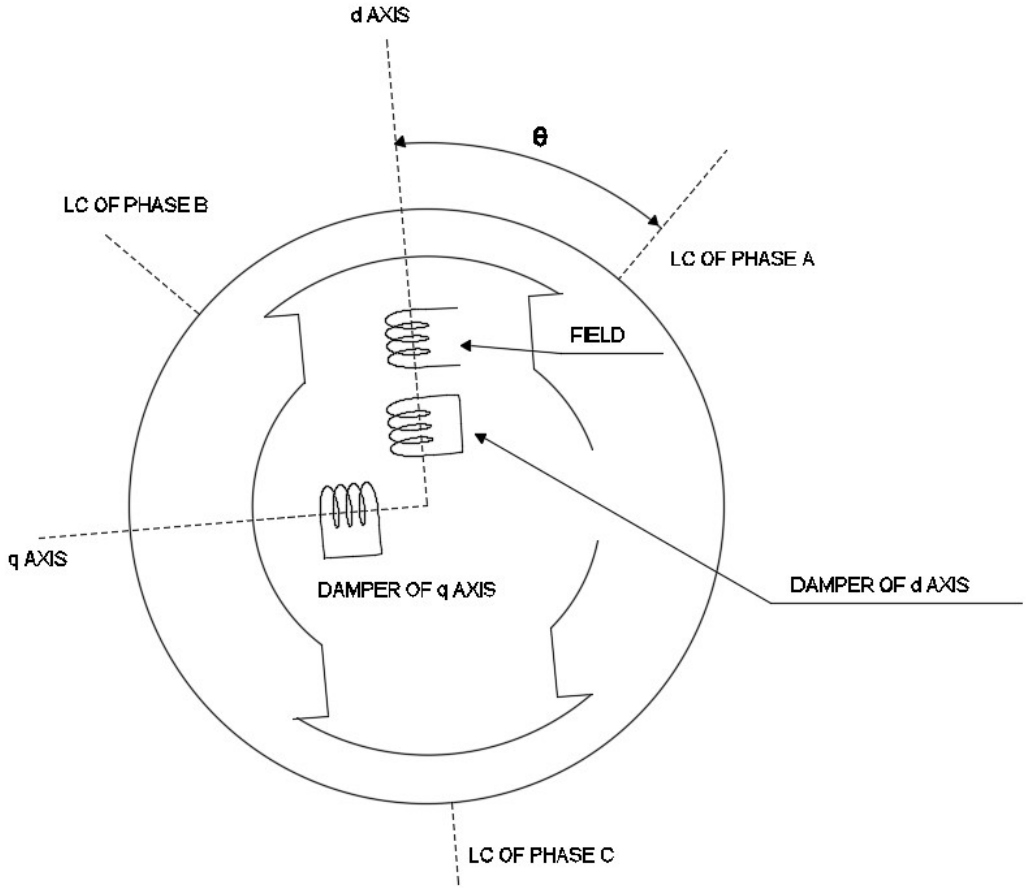

Figure 3 – Ideal Synchronous Machine [1]

There are two possible structures for the rotor: salients and round. And there are three kind of field excitation: rotative, static and mixed.

Now, considering that the stator have its own inductances per phase (2.10):

$$\begin{aligned} L_{aa} &= L_S + L_M\ cos2\theta, \\ L_{bb} &= L_S + L_M\ cos2\left(\theta - 120\right), \\ L_{cc} &= L_S + L_M\ cos2\left(\theta + 120\right), \end{aligned} \tag{2.10}$$

Where L_{aa}, L_{bb} and L_{cc} are the inductances per phase; L_S and L_M are the own and mutual inductances; θ is the angle between d-axis and phase A.

And the mutual inductances between phases of the stator on (2.11):

$$\begin{aligned} L_{ab} = L_{ba} &= -M_S - L_M\ cos2\left(\theta + 30\right), \\ L_{bc} = L_{cb} &= -M_S - L_M\ cos2\left(\theta - 90\right), \\ L_{ac} = L_{ca} &= -M_S - L_M\ cos2\left(\theta + 150\right), \end{aligned} \tag{2.11}$$

Where L_{ab}, L_{bc} and L_{ac} are the mutual inductances per phase of the stator; M_S and L_M are the own and mutual inductances; θ is the angle between d-axis and phase A.

The own field inductance (2.12):

$$L_{ff} = L_f, \tag{2.12}$$

Mutual inductance between field and the stator phases represented on (2.13),

$$\begin{aligned} L_{af} = L_{fa} &= M_F\ cos\left(\theta\right), \\ L_{bf} = L_{fb} &= M_F\ cos\left(\theta - 120\right), \\ L_{cf} = L_{fc} &= M_F\ cos\left(\theta + 120\right), \end{aligned} \tag{2.13}$$

Where L_{af}, L_{bf} and L_{cf} are the mutual inductances between field and the phases of the stator; M_f is the mutual field inductance; θ is the angle between d-axis and phase A.

Resulting on the linkage equations on phase coordinated for the phases of the stator (2.14) [1, 24]:

$$\begin{bmatrix} \lambda_a \\ \lambda_b \\ \lambda_c \end{bmatrix} = \begin{bmatrix} L_{aa} & L_{ab} & L_{ac} \\ L_{ba} & L_{bb} & L_{bc} \\ L_{ca} & L_{cb} & L_{cc} \end{bmatrix} \begin{bmatrix} i_a \\ i_b \\ i_c \end{bmatrix} + \begin{bmatrix} L_{af} \\ L_{bf} \\ L_{cf} \end{bmatrix} i_f, \tag{2.14}$$

Where λ_a, λ_b and λ_c are the linkage flux; i_a, i_b and i_c are the currents per phase, respectively. i_f is the field current.

In the field (2.15):

$$\lambda_f = L_{fa}\, i_a + L_{fb}\, i_b + L_{fc}\, i_c + L_{ff}\, i_f, \tag{2.15}$$

Beeing λ_f equals to the field linkage flux.

With the exception of L_{ff}, all the others parameters are in function of θ and of time.

2.1.3 Voltage Equations - Phase Coordinates

Considering a synchronous three windings machine on Figure 4,

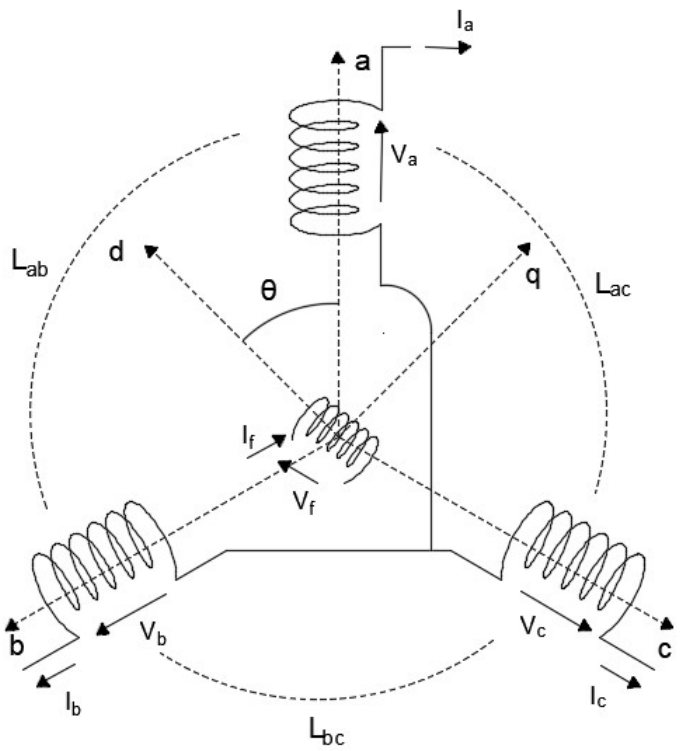

Figure 4 – Voltage Equations on Phases Coordinates

The following 4 differential equations are (2.16):

$$\begin{bmatrix} v_a \\ v_b \\ v_c \end{bmatrix} = -R \begin{bmatrix} i_a \\ i_b \\ i_c \end{bmatrix} - \begin{bmatrix} \dot{\lambda}_a \\ \dot{\lambda}_b \\ \dot{\lambda}_c \end{bmatrix}, \tag{2.16}$$

Where v_a, v_b and v_c are the voltages per phase; i_a, i_b and i_c are the currents per phase; R is the resistance per phase; $\dot{\lambda}_a$, $\dot{\lambda}_b$ and $\dot{\lambda}_c$ are the derivatives of the linked flow per phase.

Or in (2.17),

$$V_{[abc]} = -R\ I_{[abc]} - \dot{\lambda}_{[abc]}, \tag{2.17}$$

And on (2.18),

$$v_f = R_f\ i_f + \dot{\lambda}_f, \tag{2.18}$$

Where v_f and i_f are the field voltage and field current, in sequel; $\dot{\lambda}_f$ and R_f are derivative of the linked field flow and field resistance, respectively.

2.1.4 Park's Transformation

The objective of the Park's transformation is to exchange the units from the stator to the units called d and q in the rotor [25]. The equation is (2.19):

$$\phi_{[0dq]} = P\ \phi_{[abc]}, \tag{2.19}$$

Where ϕ_{0dq} and ϕ_{abc} are the flux on $0dq$ coordinates and abc, in order; P is the Park's transformation matrix (2.20).

$$[P] = \sqrt{\frac{2}{3}} \begin{bmatrix} \frac{1}{\sqrt{2}} & \frac{1}{\sqrt{2}} & \frac{1}{\sqrt{2}} \\ cos\,(\theta) & cos\,(\theta - 120) & cos\,(\theta + 120) \\ sen\,(\theta) & sen\,(\theta - 120) & sen\,(\theta + 120) \end{bmatrix}, \tag{2.20}$$

Beeing θ the angle of d-axis and phase A.

This matrix is orthogonal (2.21),

$$P^{-1} = P^T, \tag{2.21}$$

The inverse tranformation (2.22),

$$\phi_{[abc]} = P^{-1}\ \phi_{[0dq]} = P^{T}\ \phi_{[0dq]}, \tag{2.22}$$

Where P^{-1} and P^{T} is the Park's transformation inverse and transpose matrices, in sequel (2.23).

$$\left[P^{-1}\right] = \sqrt{\frac{2}{3}} \begin{bmatrix} \frac{1}{\sqrt{2}} & cos\left(\theta\right) & sen\left(\theta\right) \\ \frac{1}{\sqrt{2}} & cos\left(\theta - 120\right) & sen\left(\theta - 120\right) \\ \frac{1}{\sqrt{2}} & cos\left(\theta + 120\right) & sen\left(\theta + 120\right) \end{bmatrix}, \tag{2.23}$$

2.1.5 Linkage Flux Equations - dq Coordinates

Then, the linkage flux equations on dq coordinates is (2.24) [1]:

$$\begin{bmatrix} \lambda_0 \\ \lambda_d \\ \lambda_q \end{bmatrix} = \begin{bmatrix} L_0 & & \\ & L_d & \\ & & L_q \end{bmatrix} \begin{bmatrix} i_0 \\ i_d \\ i_q \end{bmatrix} + \sqrt{\frac{3}{2}}\ M_F\ i_f \begin{bmatrix} 0 \\ 1 \\ 0 \end{bmatrix}, \tag{2.24}$$

Where M_F is the field mutual effect; M_s is the maximum value between mutual inductances; i_0, i_d and i_q are the $0dq$ currents; λ_0 , λ_d and λ_q are the $0dq$ linked flow; L_0, L_d and L_q are the $0dq$ inductances.

And for the field linkage flux (2.25):

$$\lambda_f = L_f\ i_f + \sqrt{\frac{3}{2}}\ M_F\ i_d, \tag{2.25}$$

It can be realized that (2.25) doesn't depend on θ angle.

2.1.6 Voltage Equations - dq Coordinates

The voltage equations on dq coordinated system are expressed as (2.26) [1]:

$$\begin{bmatrix} 0 \\ v_d \\ v_q \end{bmatrix} = -R \begin{bmatrix} 0 \\ i_d \\ i_q \end{bmatrix} - \begin{bmatrix} 0 \\ \omega\ \lambda_q \\ -\omega\ \lambda_d \end{bmatrix} - \frac{d}{dt} \begin{bmatrix} 0 \\ \lambda_d \\ \lambda_q \end{bmatrix}, \tag{2.26}$$

The field voltage is expressed as in (2.27),

$$v_f = R_f \; i_f + \frac{\lambda_f}{dt}, \tag{2.27}$$

In this way, rewritting the park equations, result (2.28) to (2.30):

$$v_d = -R \; i_d - \omega \; \lambda_q - \dot{\lambda}_d, \tag{2.28}$$

$$v_q = -R \; i_q + \omega \; \lambda_d - \dot{\lambda}_q, \tag{2.29}$$

$$v_f = R_f \; i_f + \dot{\lambda}_f, \tag{2.30}$$

Beeing v_0, v_d and v_q are the $0dq$ voltages; $\dot{\lambda}_d$, $\dot{\lambda}_q$ and $\dot{\lambda}_f$ are dq derivatives of linkage flux; ω is the machine frequency.

By Park, the system of four differential equations is reduced to a three differential equations system with constant coefficients.

In balanced steady state the currents in axis dq (i_d, i_q) and in field (i_f) are constants. In addition, the linkage flux in dq axis (λ_d, λ_q) and in field (λ_f), also, are constants.

2.1.7 *P.U* Conversion

The objective of per unit conversion ($p.u$) is to express the machine equations in terms of an equivalent electric circuit. To accomplish it, a base should be chosen. On this way, when a voltage, current (or power) and frequency had been chosen, the bases to the remaining variables or circuits parameters are automatically stablished [26].

The linkage equations are in $p.u$ (2.31) and (2.32):

$$\lambda_{du} = l_u \; i_{du} + L_{adu} \; \left(i_{du} + i_{fu}\right), \tag{2.31}$$

$$\lambda_{fu} = l_{fu} \; i_{fu} + L_{adu} \; \left(i_{du} + i_{fu}\right), \tag{2.32}$$

Beeing l_u and l_{fu} the own inductances in $p.u$; L_{adu} is the mutual inductance.

Where (2.33),

$$L_{adu} = L_{mfu} = \left(KM_f\right)_u = \left(KM_F\right)_u^*, \tag{2.33}$$

In q axis, being $L_q = l + L_{aq}$, result (2.34):

$$\lambda_{qu} = l_u \; i_{qu} + L_{aqu} \; i_{qu}, \tag{2.34}$$

Considering the following voltage equations of the machine (2.35) and (2.36):

$$v_d = -R\ i_d - \frac{d\lambda_d}{dt} = \omega\ \lambda_q, \tag{2.35}$$

$$= -R\ i_d - l\ \frac{di_d}{dt} - \frac{d}{dt}\ (L_{ad}\ i_d + K\ M_F\ i_f) - \omega\ \lambda_q, \tag{2.36}$$

Dividing by the base voltage per phase (2.37):

$$V_B = R_B\ I_B = \lambda_B\ \omega_B = \frac{L_B\ I_B}{t_B} \tag{2.37}$$

it results for the voltages equations (2.38):

$$v_{du} = -R_u\ i_{du} - l_u\ \frac{di_{du}}{dt_u} - L_{adu}\ \frac{d}{dt_u}\,(i_{du} + i_{fu}) - \omega_u\ \lambda_{qu}, \tag{2.38}$$

In similar way, it gets the voltages, on $p.u$ for the q-axis and for the field (2.39) and (2.40),

$$v_{qu} = -R_u\ i_{qu} - l_u\ \frac{di_{qu}}{dt_u} - L_{aqu}\ \frac{di_{qu}}{dt_u} + \omega_u\ \lambda_{du}, \tag{2.39}$$

$$v_{fu} = R_{fu}\ i_{fu} + L_{adu}\ \frac{d}{dt_u}\,(i_{fu} + i_{du}) + l_{fu}\ \frac{di_{fu}}{dt_u}, \tag{2.40}$$

For the field, it should be considered in (2.41):

$$V_{fB} = R_{fB}\ I_{fB} = \frac{L_{fB}\ I_{fB}}{t_{fB}}, \tag{2.41}$$

And in (2.42),

$$t_B = t_{fB}, \tag{2.42}$$

2.1.8 Damped Windings

Beeing the own and the mutual inductances of the windings from the syncronous machine,

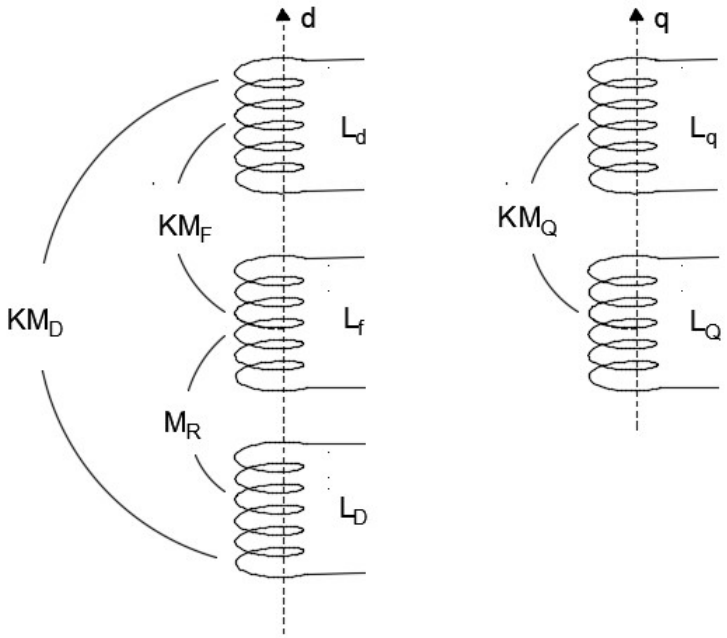

Figure 5 – Own and Mutual Inductances

In steady state the subtransients don't operate. In presence of synchronous machine oscillations, there are inductances and time constants, which are called subtransients units [1, 23, 26, 27]. Then, considering (2.43) and (2.44),

$$\begin{bmatrix} \lambda_d \\ \lambda_f \\ \lambda_D \end{bmatrix} = \begin{bmatrix} L_d & KM_F & KM_D \\ KM_F & L_f & M_R \\ KM_D & M_R & L_D \end{bmatrix} \begin{bmatrix} i_d \\ i_f \\ i_D \end{bmatrix}, \tag{2.43}$$

$$\begin{bmatrix} \lambda_q \\ \lambda_Q \end{bmatrix} = \begin{bmatrix} L_q & KM_Q \\ KM_Q & L_Q \end{bmatrix} \begin{bmatrix} i_q \\ i_Q \end{bmatrix}, \tag{2.44}$$

Where KM_D, KM_Q and M_R are the mutual indutances.

Doing the field mutual inductance equal to the d-axis mutual inductance (2.45),

$$KM_{Fu} = KM_{Du} = M_{Ru} = L_{adu}, \tag{2.45}$$

And the mutual q-axis inductance equals to the q-axis inductance (2.46),

$$KM_{Qu} = L_{aqu}, \tag{2.46}$$

It results the matrices equations of linkage flow in *p.u.* (2.47):

$$\begin{bmatrix} \lambda_{du} \\ \lambda_{fu} \\ \lambda_{Du} \end{bmatrix} = \begin{bmatrix} L_{du} & L_{adu} & L_{adu} \\ L_{adu} & L_{fu} & L_{adu} \\ L_{adu} & L_{adu} & L_{Du} \end{bmatrix} \begin{bmatrix} i_{du} \\ i_{fu} \\ i_{Du} \end{bmatrix}, \tag{2.47}$$

With $L_{Du} = l_{Du} + L_{adu}$, results (2.48).

$$\begin{bmatrix} \lambda_{qu} \\ \lambda_{Qu} \end{bmatrix} = \begin{bmatrix} L_{qu} & L_{aqu} \\ L_{aqu} & L_{Qu} \end{bmatrix} \begin{bmatrix} i_{qu} \\ i_{Qu} \end{bmatrix}, \tag{2.48}$$

With $L_{Qu} = l_{Qu} + L_{aqu}$.

On this way, the equivalents circuits are,

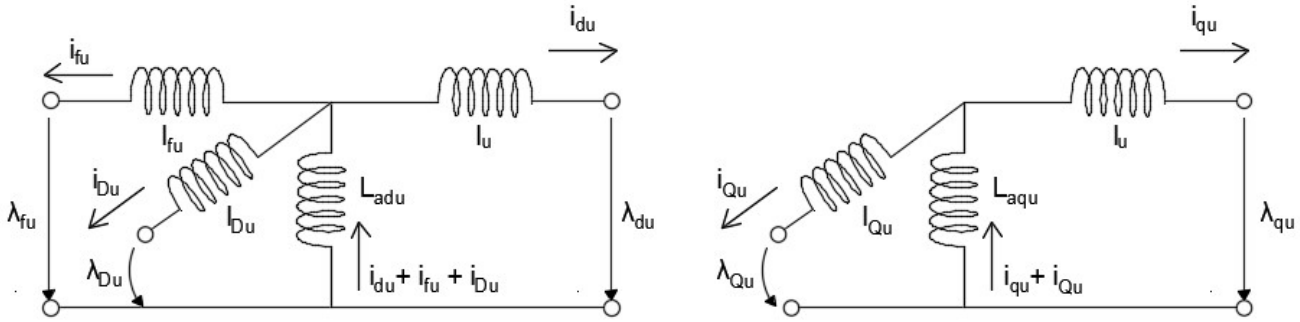

Figure 6 – Equivalents Circuits Considering Damped Windings [1]

The d-axis subtransient inductance - $L_d^{"}$ is calculated by (2.49):

$$L_d^{"} = L_d - \frac{K^2}{L_F\ L_D - M_R^2}\ \left(L_D\ M_F^2 + L_F\ M_D^2 - 2\ M_F\ M_D\ M_R\right), \tag{2.49}$$

In *p.u.* and considering $KM_{Fu} = FM_{Du} = M_{Ru} = L_{adu}$, it results (2.50):

$$L_{du}^{"} = L_{du} - \frac{L_{Du} + L_{Fu} - 2\ L_{adu}}{\frac{L_{fu}\ L_{Du}}{L_{adu}} - 1}, \tag{2.50}$$

If the total inductances are represented by (2.51) to (2.53),

$$L_{du} = l_u + L_{adu}, \tag{2.51}$$

$$L_{fu} = l_{fu} + L_{adu}, \tag{2.52}$$

$$L_{Du} = l_{Du} + L_{adu}, \tag{2.53}$$

Thus considering (2.54),

$$L_{du}^{"} = l_u + \frac{1}{\frac{1}{L_{adu}} + \frac{1}{L_{fu}} + \frac{1}{L_{Du}}}, \tag{2.54}$$

Now, the q-axis sub-transient inductance - $L_q^{"}$ is calculated on the following steps. First, knowing that the linked flow are expressed in (2.55) and in (2.56) [1, 28]:

$$\lambda_q = L_q\ i_q + K\ M_Q\ i_Q, \tag{2.55}$$
$$\lambda_Q = K\ M_Q\ i_Q + L_Q\ i_Q, \tag{2.56}$$

Calculating the total q-axis current, i_Q by (2.57):

$$i_Q = -\frac{K\ M_Q}{L_Q}\ i_q, \tag{2.57}$$

For the λ_q equation of flow in (2.59):

$$\lambda_q = L_q\ i_q + K\ M_Q\ \left(-\frac{KM_Q}{L_Q}\right)\ i_q, \tag{2.58}$$
$$\lambda_q = \left[L_q - \frac{(KM_Q)^2}{L_Q}\right]\ i_q,$$

Knowing that sub-transient inductance is calculate as $L_q^{"} = \frac{\lambda_q}{i_q}$, obtain (2.59):

$$L_q^{"} = L_q - \frac{(KM_Q)^2}{L_Q}, \tag{2.59}$$

In *p.u.*, and considering $KM_{Qu} = L_{aqu}$ result (2.60):

$$L_{qu}^{"} = L_{qu} - \frac{L_{aqu}^2}{L_{Qu}}, \tag{2.60}$$

As expressed in (2.61) and (2.62):

$$L_{qu} = l_u + L_{aqu}, \tag{2.61}$$
$$L_{Qu} = l_{Qu} + L_{aqu}, \tag{2.62}$$

Then in (2.63),

$$L_{qu}^{"} = l_u + \frac{1}{\frac{1}{L_{aqu}} + \frac{1}{l_{Qu}}} = l_u + \frac{L_{aqu}\, l_{Qu}}{L_{aqu} + l_{Qu}}, \tag{2.63}$$

The sub-transient time constant of direct axis is (2.64):

$$\tau_{du}^{"} = \frac{l_{Du} + \frac{1}{\frac{1}{L_{adu}} + \frac{1}{l_{fu}} + \frac{1}{l_u}}}{R_{Du}}, \tag{2.64}$$

And the sub-transient time constant of quadrature axis is (2.65):

$$\tau_{du}^{"} = \frac{l_{Du} + \frac{1}{\frac{1}{L_{adu}} + \frac{1}{l_{fu}} + \frac{1}{l_u}}}{R_{Du}}, \tag{2.65}$$

Where $\tau_{du}^{'}$ is the sub-transient constant of d-axis.

2.1.9 $E_q^{'}$ Model

Beeing the monophase equivalent circuit of $E_q^{'}$ model, on Figure 7,

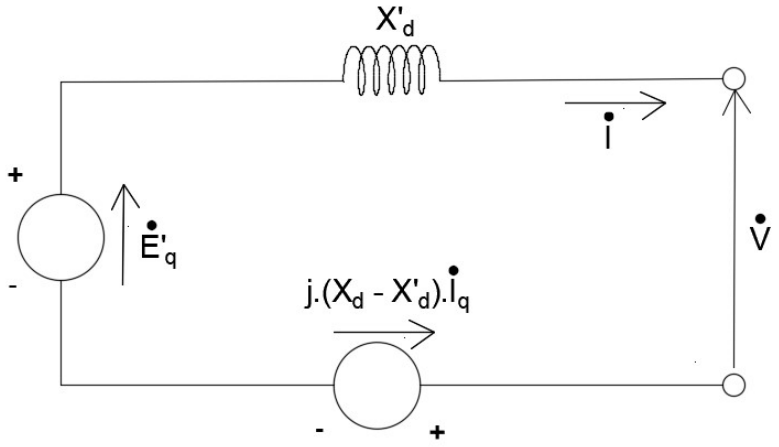

Figure 7 – Equivalent Circuit of $E_q^{'}$ Model [2]

The $E_q^{'}$ Model is represented by 3 windings, being 2 for d-axis and 1 for q-axis. The d-windings are one obtained by the dq0 transformation and one representing the machine field. The q-winding results from the $dq0$ transformation.

This Model considerate the stator resistence as zero, despise the zero sequence, the damper windings and the transformer effects voltages (2.66):

$$\frac{d\phi_d}{dt} = \frac{d\phi_q}{dt} = 0, \tag{2.66}$$

Assuming the flow linkage and voltage equations as in (2.67) to (2.71):

$$v_d = -\omega_r \ \phi_q, \tag{2.67}$$

$$v_q = \omega_r \ \phi_d, \tag{2.68}$$

$$\phi_d = -L_d \ i_d + L_{ad} \ i_f, \tag{2.69}$$

$$\phi_q = -L_q \ i_q, \tag{2.70}$$

$$\phi_f = L_f \ i_f - L_{ad} \ i_d, \tag{2.71}$$

Where, v_d and v_q are the direct and quadrature voltages, in order; ϕ_d, ϕ_q and ϕ_f are the direct, quadrature and field flow linkage, respectively; L_d, L_q and L_{ad} are the direct, quadrature and field inductances; i_d, i_q and i_f are direct, quadrature and field voltages, in sequels.

Replacing ϕ_d and ϕ_q on (2.67) and (2.68), respectively, (2.72) and (2.73):

$$v_d = \omega_r \ L_q \ i_q, \tag{2.72}$$

$$v_q = -\omega_r \ L_d \ i_d + \omega_r \ L_{ad} \ i_f, \tag{2.73}$$

Where ω_r is the actual frequency in rad/s.

Besides it, i_f is represented as in (2.74):

$$i_f = \frac{\phi_f}{L_f} + \frac{L_{ad}}{L_f} \ i_d, \tag{2.74}$$

Putting (2.74) on (2.73), it results (2.75):

$$v_q = -\omega_r \underbrace{\left(L_d - \frac{L_{ad}^2}{L_f}\right)}_{L_d^{'}} i_d + \underbrace{\omega_r \frac{L_{ad}}{L_f} \phi_f}_{e_q^{'}}, \tag{2.75}$$

With,

$L_d^{'}$ is the d-axis transient inductance;

$e_q^{'}$ is the q-axis transient voltage, proportional to the field parameters.

Then V_q is calculated as (2.76) ,

$$v_q = -\omega_r \, L_d^{'} \, i_d + e_q^{'}, \tag{2.76}$$

Remembering that X is expressed on (2.77),

$$X = \omega_r \, L, \tag{2.77}$$

Where X and $X^{'}$ are the normal and transitory rectances, respectively.

And taking the root mean square values, returns (2.78) and (2.79):

$$V_d = X_q \, I_q, \tag{2.78}$$

$$V_q = E_q^{'} - X_d^{'} \, I_d, \tag{2.79}$$

$E_q^{'}$ is the q-axis transient voltage.

In phasor values results (2.80) and (2.81),

$$\dot{V}_d = -j \, X_q \, \dot{I}_q, \tag{2.80}$$

$$\dot{E}_q^{'} = \dot{V}_q + j \, X_d^{'} \, \dot{I}_d, \tag{2.81}$$

Where V_d and V_q are the direct and quadracture voltages; X_q and $X_d^{'}$ are the quadrature and direct transient voltages; I_d and I_q are the direct and quadrature currents.

Noticing that $\dot{I}$ and $\dot{V}$ are expressed in (2.82) and in (2.83) ,

$$\dot{I} = \dot{I}_d + \dot{I}_q, \tag{2.82}$$

$$\dot{V} = \dot{V}_d + \dot{V}_q, \tag{2.83}$$

Then, applying the second Kirchhoff's law at the equivalent circuit from Figure 7 comes (2.84),

$$\dot{V} = -j\ X_q\ \dot{I}_q + \dot{E}_q^{'} \underbrace{-j\ \dot{X}_d^{'}\ \dot{I}_d - j\ X_d^{'}\ \dot{I}_q}_{-j\ X_d^{'}\ \dot{I}} + j\ X_d^{'}\ \dot{I}_q, \tag{2.84}$$

Beeing V_d and V_q expressed by (2.85) and (2.86):

$$V_d = V\ sen(\delta - \theta), \tag{2.85}$$

$$V_q = V\ cos(\delta - \theta), \tag{2.86}$$

Where δ and θ are the q-axis and bus voltages angles in relation to a reference.

Now, the direct and quadrature currents in (2.78) and in (2.79) are expressed as in (2.87) and in (2.88),

$$I_d = \frac{E_q^{'} - V\ cos(\delta - \theta)}{X_d^{'}}, \tag{2.87}$$

$$I_q = \frac{V\ sen(\delta - \theta)}{X_q}, \tag{2.88}$$

Define, on this moment, the electromagnetic conjugate considering the simplification at the beginning on this model presentation. Therefore, it's possible to get for electrical power in (2.89):

$$P_e = V_d\ I_d + V_q\ I_q, \tag{2.89}$$

Thus in (2.90),

$$\begin{aligned} P_e &= X_q\ I_q\ I_d + (E_q^{'} - X_d^{'}\ I_d)\ I_q, \\ &= E_q^{'}\ I_q + (X_q - X_d^{'})\ I_d\ I_q, \end{aligned} \tag{2.90}$$

Deducting the state equation for V_f (2.91),

$$v_f = R_f \; i_f + \frac{d\phi_f}{dt}, \tag{2.91}$$

Where R_f is the field resistence.

Multiplying (2.91) for $\omega_r \; \frac{L_{ad}}{R_f}$, it results (2.92) and (2.93):

$$\underbrace{\omega_r \; \frac{L_{ad}}{R_f} \; v_f}_{e_{fd}} = \omega_r \; \frac{L_{ad}}{R_f} \; R_f \; i_f + \frac{d}{dt}\left(\omega_r \; \frac{L_{ad}}{R_f} \; \phi_f\right), \tag{2.92}$$

$$e_{fd} = \underbrace{\omega_r \; L_{ad} \; i_f}_{eq} + \frac{L_f}{R_f} \; \frac{d}{dt} \underbrace{\left(\omega_r \; \frac{L_{ad}}{L_f} \; \phi_f\right)}_{e_q^{'}}, \tag{2.93}$$

Where v_f is the field voltage.

Therefore, e_{fd} is obtained as in (2.94),

$$e_{fd} = e_q + \underbrace{\frac{L_F}{R_F}}_{\tau_{d0}^{'}} \; \frac{de_q^{'}}{dt}, \tag{2.94}$$

Rearranging and using effective values, comes (2.95):

$$\frac{dE_q^{'}}{dt} = \frac{1}{\tau_{d0}^{'}} \; (E_{fd} - E_q), \tag{2.95}$$

Where:

E_{fd} is the proportional voltage to the field voltage;

E_q is the q-axis voltage

$\tau_{d0}^{'}$ is the transient time constant of d-axis.

Remembering for v_q (2.96),

$$v_q = -\omega_r \; L_d \; i_d + \underbrace{\omega_r \; L_{ad} \; i_f}_{e_q}, \tag{2.96}$$

Taking into account *rms* values, it results (2.97) :

$$V_q = E_q - X_d \; I_d, \tag{2.97}$$

But, from (2.78) and (2.79), it arrives on (2.98):

$$V_q = E_q^{'} - X_d^{'} \; I_d, \tag{2.98}$$

Soon in (2.99),

$$E_q = E_q^{'} + (X_d - X_d^{'}) \; I_d, \tag{2.99}$$

Finally [1, 8, 29], results (2.100),

$$\frac{dE_q^{'}}{dt} = \frac{1}{\tau_{d0}^{'}} \left(E_{fd} - E_q^{'} - (X_d - X_d^{'}) \; I_d \right), \tag{2.100}$$

E_{fd} will be constant if there is no excitation system.

The rotor oscillation equations will be expressed in (2.101) and in (2.102) [8, 13, 20, 30]:

$$\frac{d\delta}{dt} = \omega_r - \omega_s = \Delta\omega_r, \tag{2.101}$$

$$\frac{d\omega_r}{dt} = \frac{1}{2 \; H} \; (T_m - P_e - D_m \; \Delta\omega_r), \tag{2.102}$$

Considering the electromagnetic conjugate is (2.103),

$$\frac{d\omega_r}{dt} = \frac{1}{2 \; H} \; \left[T_m - E_q^{'} \; I_q - (X_q - X_q^{'}) \; I_d \; I_q - D_m \; \Delta\omega_r \right], \tag{2.103}$$

The algebraic equations become (2.104) and (2.105):

$$I_d = \frac{E_q^{'} - V \; cos(\delta - \theta)}{X_d^{'}}, \tag{2.104}$$

$$I_q = \frac{V \; sen(\delta - \theta)}{X_q}. \tag{2.105}$$

Being the direct reactance, X_d, equal to the quadrature reactance, X_q for the round rotor machines.

The $E_q^{'}$ Model is defined by the equations (2.100), (2.101), (2.102) and (2.103) and the algebraic equations (2.104) and (2.105).

2.1.10 Classical Model

The Classical Model is a simplification of the Constant $E_q^{'}$ Model [31]. Taking into account the equation (2.100), comes (2.106):

$$E_{fd} = E_q = E_q^{'} + \left(X_d - X_d^{'}\right)\ I_d, \tag{2.106}$$

In this way, the equation (2.106) and the differential equations (2.101), (2.102) and (2.103) and the algebraic equations (2.104) and (2.105) represent the constant $E_q^{'}$ model.

Now, again, the classical model is a particular case of the $E_q^{'}$ model, considering the following equalities represented in (2.107), (2.108) and (2.109):

$$X_d = X_q, \tag{2.107}$$

$$X_{fd} = X_q = X_q^{'}, \tag{2.108}$$

$$X_d = X_d^{'}. \tag{2.109}$$

Where X_d and X_q are the direct and quadrature axis reactances, respectively; X_{fd} is the field reactance; And $X_d^{'}$ and $X_q^{'}$ are the direct and quadrature axis transitory reactances, respectively.

Then for $\dot{\omega}_r$ in (2.110),

$$\frac{d\omega_r}{dt} = \frac{1}{2\ H}\ \left[T_m - E_q^{'}\ \frac{V}{X_d^{'}}\ sen\left(\delta - \theta\right) - D\ \Delta\omega_r\right], \tag{2.110}$$

As results, the classical model equations are (2.101), (2.102), (2.103) and (2.110). And its equivalent circuit is:

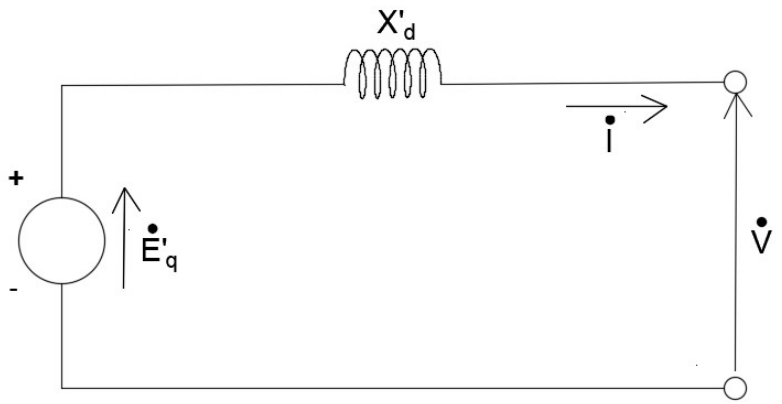

Figure 8 – Classical Model Equivalent Circuit [2]

It can be concluded that according to [8], the classical model is a simple model considers constant the quadrature axis transient voltage, $\dot{E}_q^{'}$. Resulting in the elimination of one differential equation linked to the electrical characteristics of the machine, resulting on a system with two ordinal differential equations [12, 32]. Besides it, another simplification is making the direct transient reactance ($X_d^{'}$) equal and constant to the quadrature axis reactance ($X_q^{'}$). This mathematical model is used to represent far away machines from the principal area and without the representation of the excitation systems and voltage regulators.

3 New Synchronous Machine Modeling

Considering the representation of the classical model in complex plane, the first step is writting mathematically all state real variables in complex domain. In second step, the developments of the state equation, $f_1 = \frac{d\alpha}{dt}$, and the algebraic equations are presented.

3.1 Classical Model

3.1.1 State Complex Equation

The complex state variable, α, in classical model has two parts, as expressed in (3.1). The real component is represented by the angle of each machine, "δ". And the imaginary component is represented by the frequency variation, "$\Delta\omega$". Then, putting together those two state variables on just one complex variable. And realizing that this variable in complex plane, "α", doesn't have any physical meaning but only mathematical one. Beginning the development and observing that the symbol "$*$" up the variable means conjugate,

$$\alpha = \delta + j\ \Delta\omega, \tag{3.1}$$

Where, δ and $\Delta\omega$ are the rotor angle in radians and synchronous rotor speed deviation in radians/s of every machine, respectively.

Considering the equations (3.2) and (3.2) in complex plane for δ and $\Delta\omega$,

$$\delta = \quad 0.5\ \left(\alpha + \alpha^*\right), \tag{3.2}$$

$$\Delta\omega = j\ 0.5\ \left(\alpha^* - \alpha\right), \tag{3.3}$$

Taking the derivative of (3.1) as f_1 represented by (3.4),

$$f_1 = \frac{d\alpha}{dt} = \frac{d\delta}{dt} + j\ \frac{d\omega}{dt}, \tag{3.4}$$

The real derivatives of $\frac{d\delta}{dt}$ and $\frac{d\omega}{dt}$ are, in $p.u$, (3.5) and (3.6), respectively:

$$\frac{d\delta}{dt} = \omega - \omega_s = \Delta\omega, \tag{3.5}$$

$$\frac{d\omega}{dt} = \frac{\omega_s}{2\ H}\ (T_m - P_e - D\ \Delta\omega), \tag{3.6}$$

Where ω and ω_s are respectively actual and synchronous rotor speed in radians/s; T_M, H and D denote the mechanical power input conjugate, the inertia constant and the damping factor; P_e is the real power output, respectively.

Replacing (3.3) in (3.5) and in (3.6), results (3.7) and (3.8),

$$\frac{d\delta}{dt} = j\ 0.5\ \ (\alpha^* - \alpha)\,, \tag{3.7}$$

$$\frac{d\omega}{dt} = \frac{\omega_s}{2\ H}\ \ [T_M - P_e - D\ \ (j\ 0.5\ \ (\alpha^* - \alpha))]\,. \tag{3.8}$$

Substituting (3.7) and (3.8) in (3.4), comes for f_1 (3.9),

$$f_1 = j\ 0.5\ \ (\alpha^* - \alpha) + j\ \frac{\omega_s}{2\ H}\ \ [T_M - P_e - D\ \ (j\ 0.5\ \ (\alpha^* - \alpha))]\,, \tag{3.9}$$

Organizing the state complex variables α and α^*, obtains (3.10):

$$\frac{d\alpha}{dt} = \underbrace{-0.5\ \left(\frac{D\ \omega_s}{2H} + j\right)}_{A_1}\ \alpha + \underbrace{0.5\left(\frac{D\ \omega_s}{2H} + j\right)}_{-A_1}\ \alpha^* + \underbrace{j\ \frac{\omega_s}{2H}}_{A_2}\ T_m + \underbrace{\left(-j\ \frac{\omega_s}{2H}\right)}_{-A_2}\ P_e, \tag{3.10}$$

Getting the complex equation for f_1 (3.11),

$$\frac{d\alpha}{dt} = A_1\ (\alpha - \alpha^*) + A_2\ (T_m - P_e). \tag{3.11}$$

Nonetheless, recalling that the electric power can be expressed as 3.16. And replacing (3.16) into (3.11) allows to obtain the dynamic equation (3.12) formulated in the complex domain for the classical model of a synchronous machine.

$$\frac{d\alpha}{dt} = A_1\ (\alpha - \alpha^*) - 0.5\ A_2\ (S_e + S_e^*) + A_2\ T_m. \tag{3.12}$$

Observing that in (3.12) the voltage and turbine regulators models are not included. Consequently, the mechanical power is a constant, making the previous equation dependent exclusively of complex variables.

On this way, implementing and initializing of the real ODEs, in SIMULINK representation the real state equations are shown in Fig. 9 and Fig. 10, respectively,

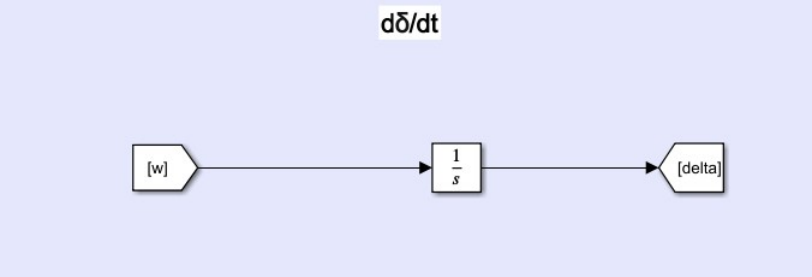

Figure 9 – Real State Equation of δ for the 9-Bus IEEE System

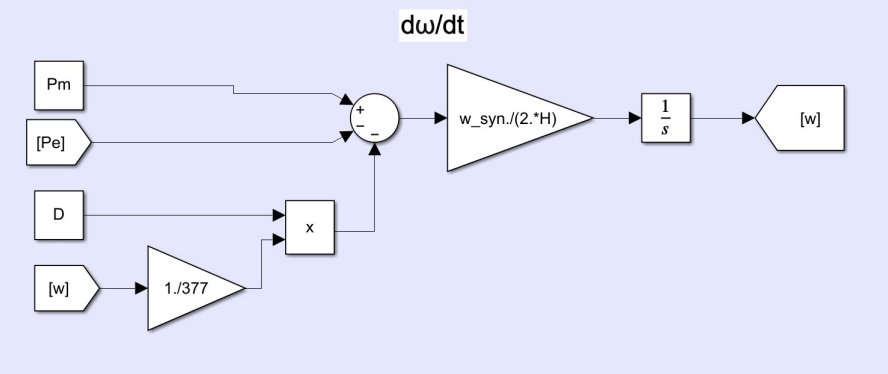

Figure 10 – Real State Equation of ω for the 9-Bus IEEE System

In the same way for complex plane, it was initialized and implemented an ODE, as explained on previous chapter, on SIMULINK, representing the complex state equation, as seen on Figure 11,

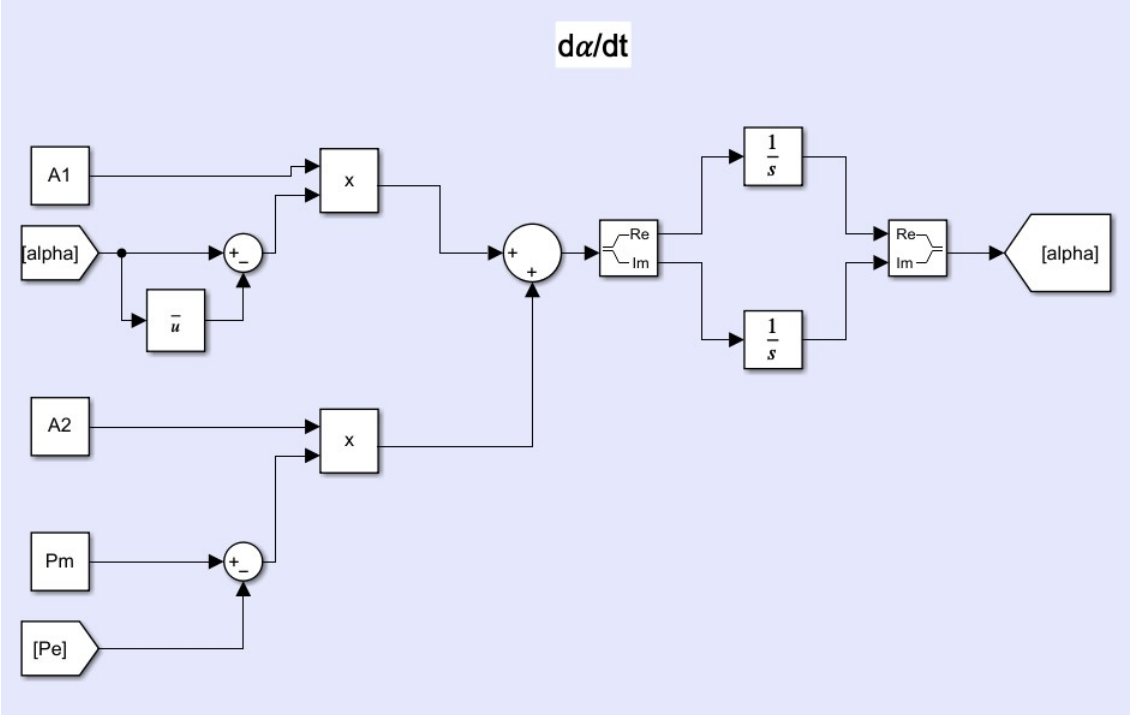

Figure 11 – Complex State Equation of α for the 9-Bus IEEE System

3.1.2 Algebraic Complex Equations

Taking into account that the algebraic equation in its complex domain have a real and an imaginary parts. The algebrac equations for the voltage, current and power are (3.13), (3.14) and (3.16), respectively,

$$\overline{E} = E\angle\delta = V_t\angle\theta_t - jX_d^{'} \cdot \overline{I}_a, \tag{3.13}$$

$$\overline{I}_i = \sum_{k=1}^{n} \overline{Y}_{ik}^{red} \cdot \overline{E}_k = \sum_{k=1}^{n} Y_{ik}^{red} E_k \angle(\gamma_{ik} + \delta_k), \tag{3.14}$$

$$Se_i = \overline{E}_i \ \overline{I}_i^* = \overline{E}_i \ \left[\sum_{k=1}^{n} \overline{Y}_{ik}^{red} \cdot \overline{E}_k\right]^*, \tag{3.15}$$

$$Pe = \Re(Se) = 0.5 \ (S_e + S_e^*) = \sum_{k=1}^{n} E_i E_k Y_{ik}^{red} \cos(\delta_i - \delta_k - \gamma_{ik}), \tag{3.16}$$

Where δ is the angle between the phase A and d-axis. Observing that the loads characteristics vary significantly with time of the day, day of week and weather [33]. So, on this work the loads will be represented as constant impedance, as on [34].

Implementing on SIMULINK the complex and real algebraic equations for voltage are presented on Figures 12 and 15. Taking into consideration that the complex algebraic equations for current and power are the same from real plane,

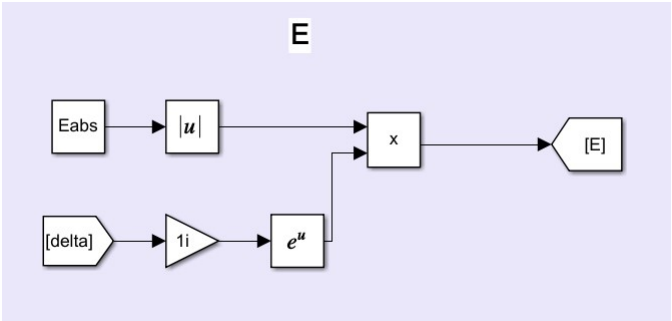

Figure 12 – Real Algebraic Equation of Voltage for the 9-Bus IEEE System

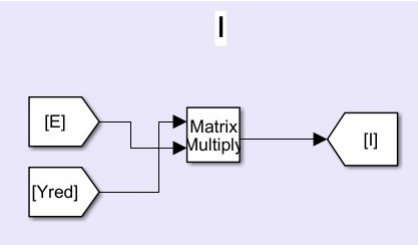

Figure 13 – Real Algebraic Equation of Current for the 9-Bus IEEE System

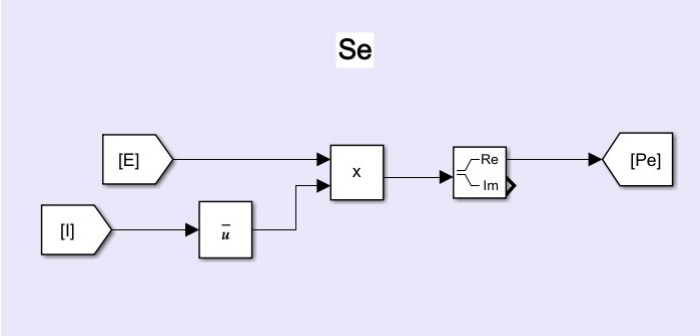

Figure 14 – Real Algebraic Equation of Power for the 9-Bus IEEE System

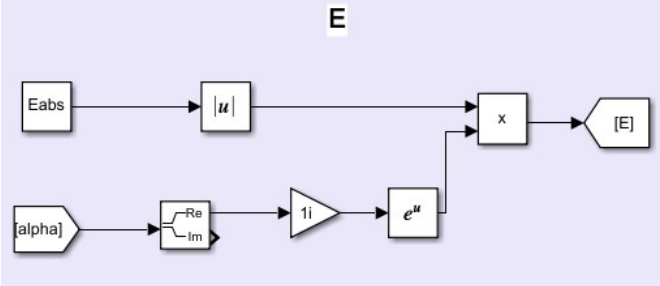

Figure 15 – Complex Algebraic Equation of Voltage for the 9-Bus IEEE System

Keeping in mind that Kron reduction is used to simplify the analysis of multi-machine power systems under certain steady state assumptions [35]. The reduced matrix, Y_{red}, for the complex and real planes, is represented on Figure 16,

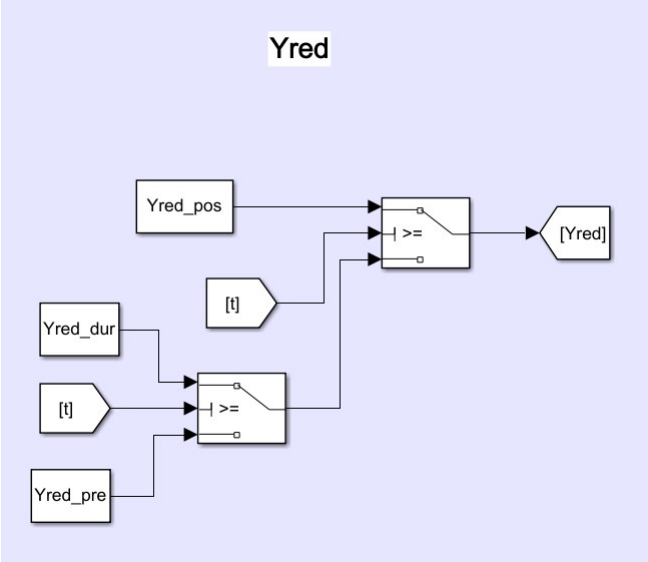

Figure 16 – Reduced System Matrix for the Complex and Real Planes of the 9-Bus IEEE System

4 Numerical Results

In this chapter presents the dynamic results in the complex and real planes of the power system through test systems. The machine dynamic equations were formulated on real plane on previous studies. Initially, it shows a first study case. After it, a second study case is shown. Finally, it presents a comparative of efficiency time between these two systems in complex and in real domains.

The simulations were run on MATLAB and SIMULINK, according to [36, 37], with the validations on ORGANON (software from a consulting and P&D company called HPPA, made for ONS) [38, 39]. The test systems analyzed were IEEE 9 and 39 bus, also known as New England. The numerical results were performed on a Intel(R) Core i5 CPU 2,50 GHz, 8 GB of RAM and operating system of 64 bits. It uses the flat start voltages profiles to initialize the state variables.

4.1 Case Study: 9-Bus System

4.1.1 Data Preprocessing

Considering the IEEE system for the first case test beeing the 9 bus, as seen on Figure 17, with the parameters [12] [40] where its data can be seen on Appendix A.

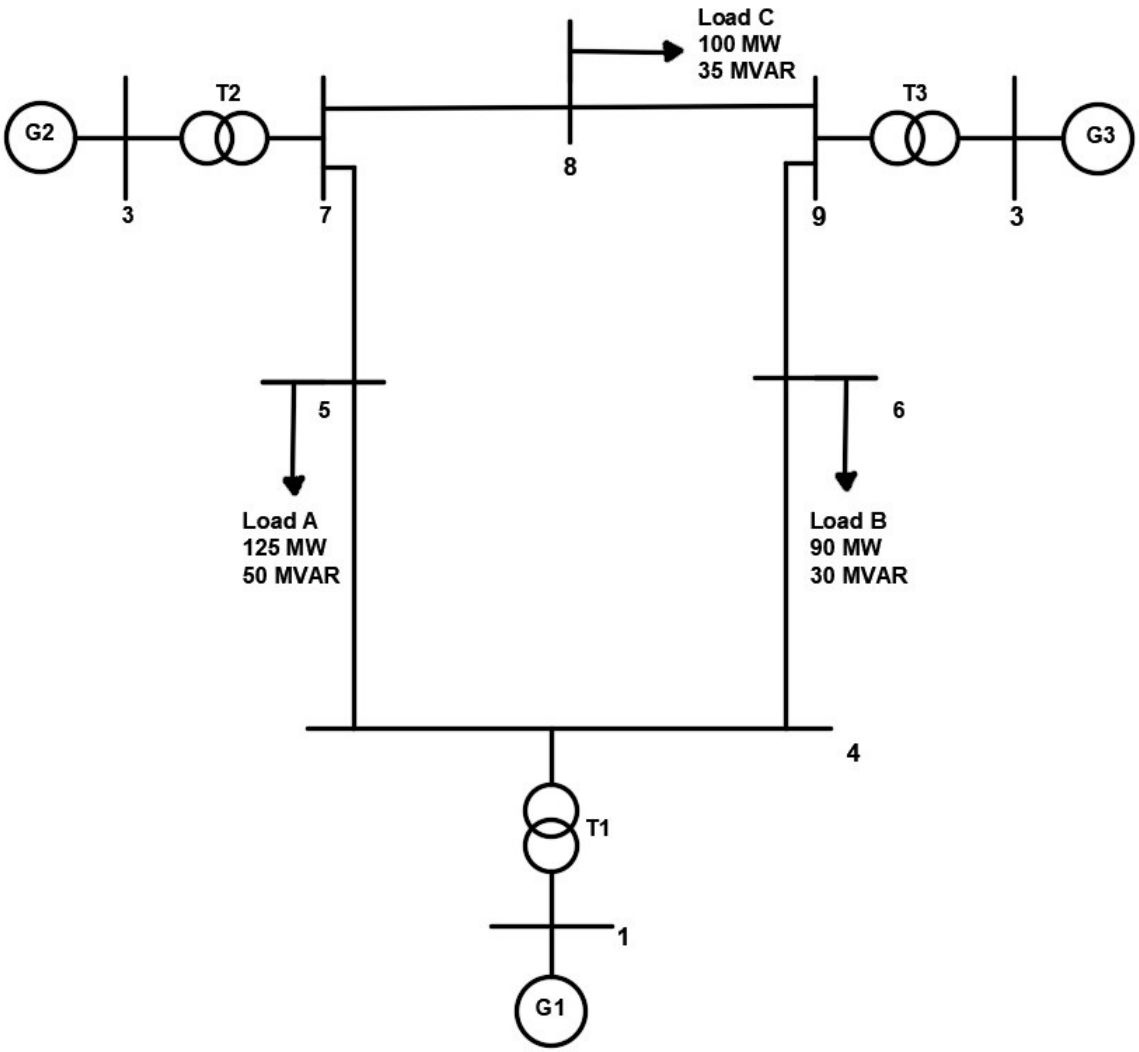

Figure 17 – 9-Bus IEEE System [3]

First, it used the Newton-Raphson algorithm to get the power flow solution [41]. The tolerance adopted on SIMULINK was of 10^{-5} [16]. And the one adopted in ORGANON was 10^{-3}. Then, the table 1 is the output report for the bus. The used algorithm came out with the same results presented on a Matlab electrical engineering library, called Matpower for this system [42].

Table 1 – Power Flow for IEEE - 9 Bus System

Bus ♯	$V\,[p.u]$	$Ang\,[°]$
1	$1,040$	$0,000$
2	$1,025$	$8,839$
3	$1,025$	$4,619$
4	$1,026$	$-2,217$
5	$0,996$	$-3,989$
6	$1,013$	$-3,687$
7	$1,026$	$3,717$
8	$1,016$	$0,727$
9	$1,032$	$1,967$

The power flow reports were used as input data to initialize the algebraic and state variables of the differential equations described on the previous chapter.

Now, it was considered the following disturb applied near bus 8 on 0,1s,

Table 2 – Disturb on IEEE - 9 Bus System

Type	Location	Nearby Bus	Disturb Duration	Fault Elimination
$SC3P$	$Line_{(8-9)}$	8	$300ms$	Open $Line_{(8-9)}$

But, the numerical results will be shown just for the δ that gives the biggest difference with ORGANON according to the table 3,

Table 3 – Differences of δ

δ_{21}	δ_{31}	δ_{12}	δ_{32}	δ_{13}	δ_{23}
$0,46°$	$1,09°$	$0,60°$	$1,73°$	$1,47°$	$2,28°$

Thefore, it will be obtained the results for the machine 2, considering the machine 3 on system reference of the IEEE 9-bus system, because the biggest difference occurred at $3.5s$. On this case, the ω for each machine are presented on Figures 18, 19 and 20

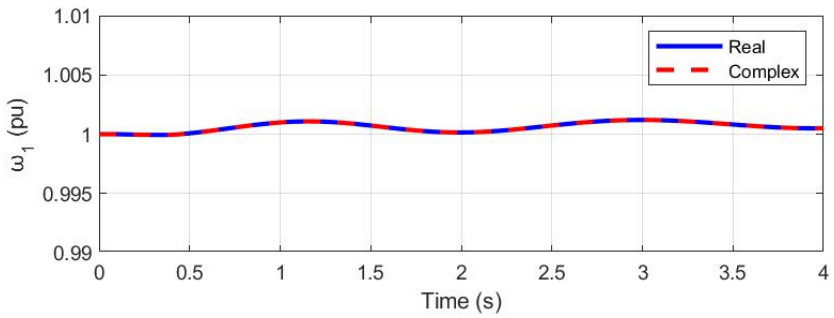

Figure 18 – ω_1 for the Machine 1 of the 9-Bus IEEE System

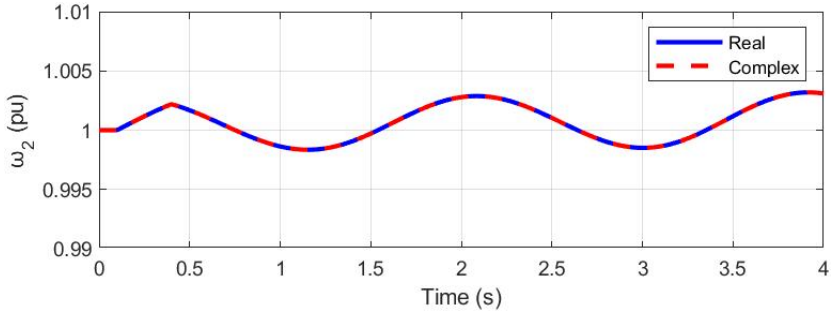

Figure 19 – ω_2 for the Machine 2 of the 9-Bus IEEE System

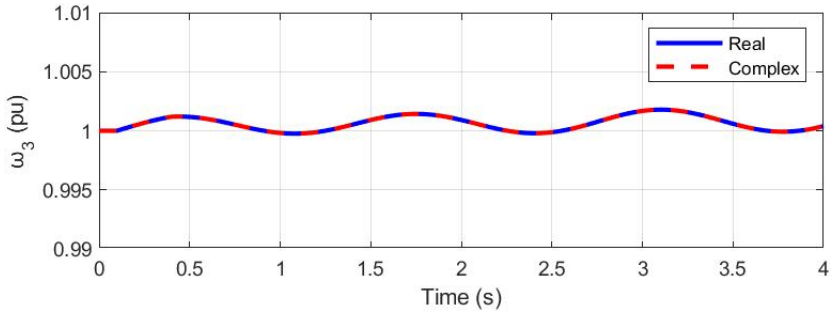

Figure 20 – ω_3 for the Machine 3 of the 9-Bus IEEE System

For the previous MATLAB graphics obtained from fix Runge-Kutta integration method, called $ODE4$, the complex variable ω tracks the real variable for each machine. These were awaited results and it can be resumed on a comparative real graphic on Figure 21,

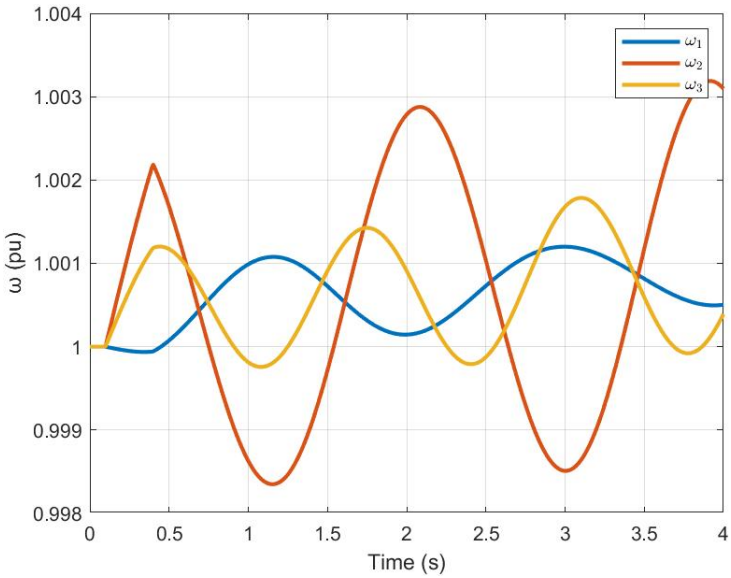

Figure 21 – Comparative for ω of Each Machine of the 9-Bus IEEE System

So, comparing the ω_2 got from SIMULINK, using another 3 variable integration methods, $ODE45$, $ODE113$ and $ODE23t$ with ORGANON for this system,

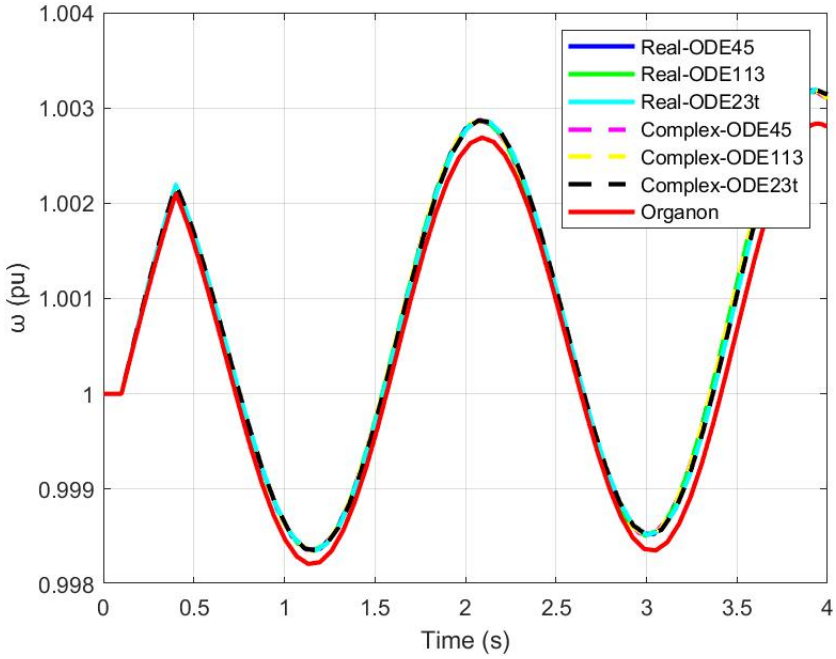

Figure 22 – ω_2 of Machine 2 on SIMULINK and on ORGANON

Looking on Figure 22 and using the 3 integration methods it verifies that the state variable of the second machine. ω_2, formulated on complex and real planes implemented, is dynamically equal to the validation program, ORGANON. Adicionally, it's observed for this variable a difference of 10^{-15} $p.u$ between complex and real planes on every method.

According to the Figure 22 and to the Table 4, on 3,95s, the ω_2 using ODE23t from SIMULINK, is the closest method, with variable integration step, to the same variable got from ORGANON.

On this time, it will be shown the result for δ_{23},

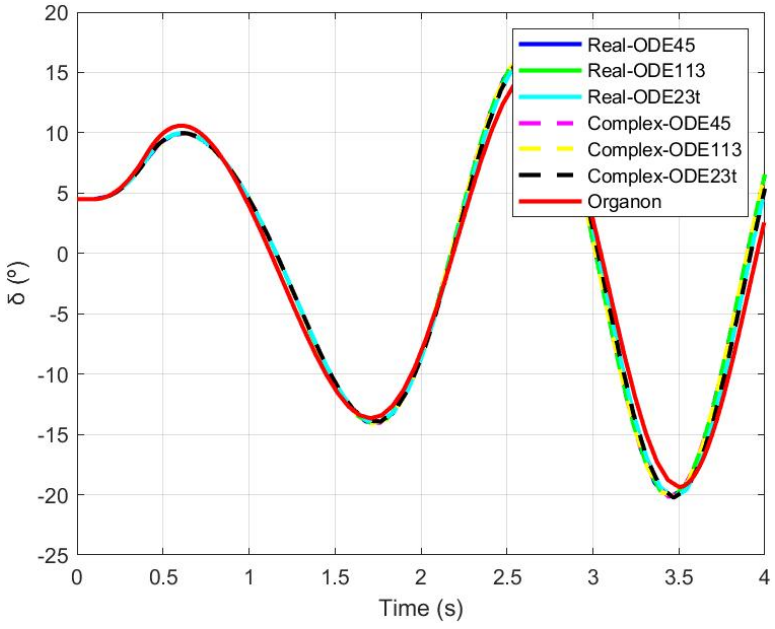

Figure 23 – δ_{23} of the 9-Bus IEEE System

The difference between this variable in complex and in real planes is 10^{-13} degrees. It's a small value, meaning the results are similar.

How it can be seen on Figure 23, until the applying of short circuit the angle δ_{23} keeps continuous because it's steady state. After 0,1s, the machine 2 angle having a not convergent comportment, holding it same after removing the fault in 0,4s. Both graphics in real and complex planes have the same dynamics with the graphic of ORGANON for this state variable, considering the trapezoidal integration method. The other 2 integration methods ($ODE45$ and $ODE113$) have the same dynamics, as seen on Figure 23. To compare the closest method to approach the ORGANON result for this variable, it was chose the time 2,62s. Therefore, the trapezoidal method, $ODE23t$, has the lowest value of $1,64°$, between all variable step integration methods and ORGANON, on this instant, how observed on Table 4.

Table 4 – Values of Simulink Integration Methods and of Organon - 9-Bus IEEE

9 - Bus IEEE System							
IM	Variables				ORGANON	Variables	
	Real		Complex			Real	
	$\delta_{23}^{\circ}\,(t = 2,62s)$	$\omega_2\,(t = 3,95s)$	δ_{23}°	ω_2		δ_{23}°	ω_2
$ODE45$	$16,36$	$1,00315$	$16,36$	$1,00315$			
$ODE113$	$16,38$	$1,00314$	$16,38$	$1,00314$		$14,7$	$1,0028$
$ODE23t$	$16,34$	$1,00313$	$16,34$	$1,00313$			

Observing the dynamics of δ_{23} and ω_2 when using the fix and variable integration step methods, $ODE4$, $ODE45$, $ODE23t$ and $ODE113$,respectively, the one that represent better is the fix integration step method, with the same used absolute and relative tolerances in ORGANON. These integration methods are explained on appendix C and D.

It's important to note the convergence of the IEEE 9-bus system on Figure 24,

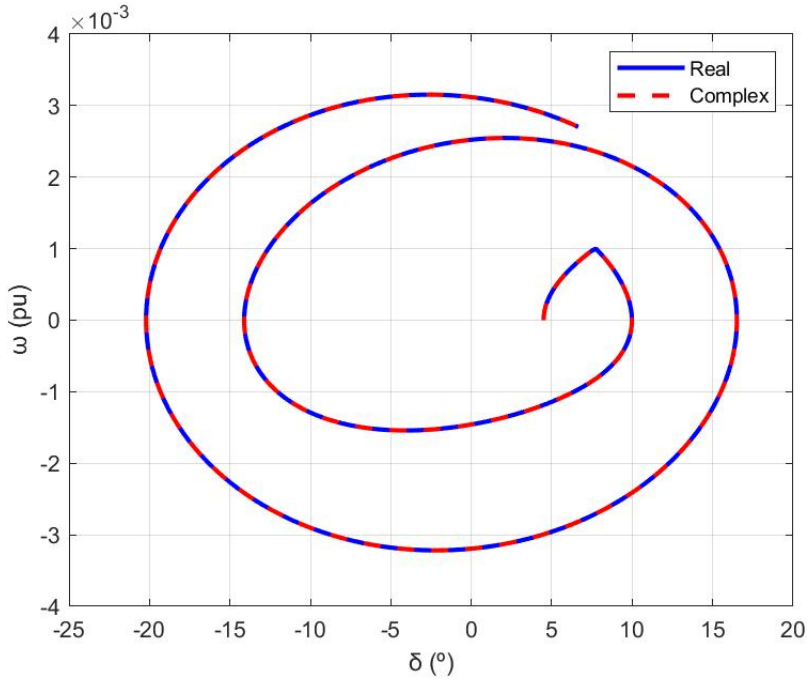

Figure 24 – Convergence of δ During the Event on the 9-Bus IEEE System

As seen on last graphic, initially, the δ and ω has its values on steady state. After a short circuit, the both state variables change its operating point until to achieve a new diverged operational point on 4s. It can conclude that the formulations in real and in complex planes have the same operating dynamic. In this way, the theory presented on [1, 8, 27, 43, 44] matches with this first study case.

4.2 Case Study: 39-Bus System

4.2.1 Data Preprocessing

Observing the known IEEE test-system of 39 bus, called New-England, as seen on Figure 25, with the parameters and system data can be seen on Appendix B,

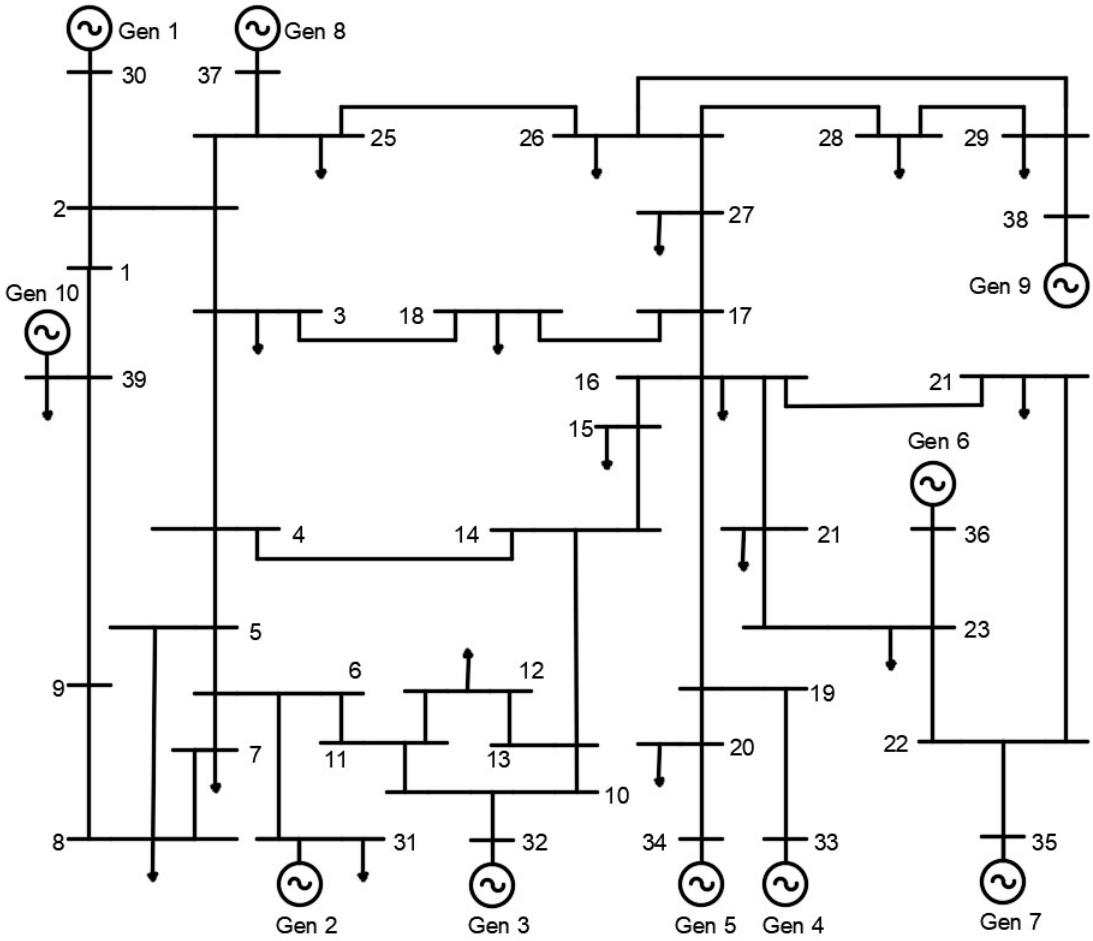

Figure 25 – 39-Bus IEEE System [4]

Firstly, using the Newton-Raphson algorithm to get the power flow solution [41]. The tolerance adopted in SIMULINK was of 10^{-5} [16]. And the tolerance considered in ORGANON was of 10^{-3} for the power flow.Then, the table 5 is the output report for the bus. The used algorithm came out with the same results presented on a Matlab library, called Matpower, for this system [42].

Table 5 – Power Flow for IEEE - 39 Bus System

Bus ♯	$V\,[p.u]$	$Ang\,[^\circ]$
1	$1,036$	$-8,464$
2	$1,037$	$-5,714$
3	$1,020$	$-8,644$
4	$0,996$	$-9,681$
5	$0,999$	$-8,675$
6	$1,002$	$-8,006$
7	$0,991$	$-10,204$
8	$0,990$	$-10,701$
9	$1,020$	$-10,392$
10	$1,012$	$-5,461$
11	$1,008$	$-6,325$
12	$0,995$	$-6,284$
13	$1,009$	$-6,136$
14	$1,004$	$-7,707$
15	$1,005$	$-7,784$
16	$1,020$	$-6,199$
17	$1,023$	$-7,341$
18	$1,020$	$-8,275$
19	$1,045$	$-0,988$
20	$0,989$	$-1,992$
21	$1,016$	$-3,712$
22	$1,030$	$0,907$
23	$1,024$	$0,707$
24	$1,024$	$-6,074$
25	$1,049$	$-4,426$
26	$1,045$	$-5,584$
27	$1,029$	$-7,563$
28	$1,046$	$-2,048$
29	$1,047$	$0,725$
30	$1,027$	$-3,217$
31	$0,982$	$0,000$
32	$0,983$	$2,575$
33	$0,997$	$4,241$
34	$1,012$	$3,206$
35	$1,029$	$6,063$
36	$1,033$	$8,971$
37	$1,027$	$2,408$
38	$1,026$	$7,805$
39	$1,020$	$-10,114$

The power flow reports were used as input data to initialize the algebraic and state variables of the differential equations described on the previous chapter.

In this way, implementing and initializing the real ODEs, in SIMULINK, repre-

senting the real state and algebraic equations result the same Figures 9, 10, 12, 13 and 14, respectively. for the first test case. Equally, doing the same process for the ODE in complex plane, in SIMULINK, representing the complex state and algebraic equations result the Figures 11 and 15 of the IEEE 9-bus. And taking into consideration that the others complex algebraic variables, current and electric power, are represented on the same way, in Figures 13 and 14 for complex plane of IEEE 9-bus system.

Considering the following disturb near to Bus 15 applied on $0,1$s,

Table 6 – Disturb on IEEE - 39 Bus System

Type	Location	Nearby Bus	Disturb Duration	Fault Elimination
$SC3P$	$Line_{(14-15)}$	15	$300ms$	Open $Line_{(14-15)}$

However, the numerical results will be shown just for the δ that gives the biggest difference with ORGANON according to the table 7,

Table 7 – Differences of δ

δ_{21}	δ_{31}	δ_{41}	δ_{51}	δ_{61}	δ_{71}	δ_{81}	δ_{91}	δ_{10-1}
$0,86°$	$0,87°$	$3,09°$	$3,24°$	$3,24°$	$3,78°$	$1°$	$3,90°$	$3,22°$
δ_{12}	δ_{32}	δ_{42}	δ_{52}	δ_{62}	δ_{72}	δ_{82}	δ_{92}	δ_{10-2}
$0,85°$	$0,78°$	$2,97°$	$3,07°$	$2,67°$	$3,70°$	$1,31°$	$3,85°$	$3,24°$
δ_{13}	δ_{23}	δ_{43}	δ_{53}	δ_{63}	δ_{73}	δ_{83}	δ_{93}	δ_{10-3}
$0,85°$	$0,78°$	$2,26°$	$2,62°$	$3,04°$	$3,26°$	$1,21°$	$3,70°$	$3,25°$
δ_{14}	δ_{24}	δ_{34}	δ_{54}	δ_{64}	δ_{74}	δ_{84}	δ_{94}	δ_{10-4}
$3,08°$	$2,68°$	$2,56°$	$2,01°$	$0,54°$	$0,75°$	$2,42°$	$1,77°$	$3,83°$
δ_{15}	δ_{25}	δ_{35}	δ_{45}	δ_{65}	δ_{75}	δ_{85}	δ_{95}	δ_{10-5}
$2,81°$	$3,15°$	$2,66°$	$3,03°$	$0,22°$	$0,91°$	$2,13°$	$2,40°$	$3,62°$
δ_{16}	δ_{26}	δ_{36}	δ_{46}	δ_{56}	δ_{76}	δ_{86}	δ_{96}	δ_{10-6}
$2,83°$	$2,47°$	$2,93°$	$0,52°$	$0,75°$	$0,20°$	$2,10°$	$1,89°$	$3,84°$
δ_{17}	δ_{27}	δ_{37}	δ_{47}	δ_{57}	δ_{67}	δ_{87}	δ_{97}	δ_{10-7}
$3,79°$	$3,69°$	$3,33°$	$0,78°$	$0,91°$	$0,49°$	$2,51°$	$1,90°$	$3,23°$
δ_{18}	δ_{28}	δ_{38}	δ_{48}	δ_{58}	δ_{68}	δ_{78}	δ_{98}	δ_{10-8}
$1,01°$	$1,31°$	$1,21°$	$2,44°$	$2,15°$	$2,10°$	$2,76°$	$2,21°$	$3,17°$
δ_{19}	δ_{29}	δ_{39}	δ_{49}	δ_{59}	δ_{69}	δ_{79}	δ_{89}	δ_{10-9}
$1,77°$	$3,04°$	$3,69°$	$1,68°$	$2,06°$	$1,88°$	$1,89°$	$2,43°$	$3,11°$

Therefore, it will be shown the results for the machine 9, considering the machine 1 on system reference of the IEEE 39-bus system and using Runge-Kutta fix integration method, $ODE4$, because the biggest angle difference between ORGANON and the classical model, 3.90°, occured at $3.2s$. In this case, the ω for each machine are presented on Figures 26, 27, 28, 29, 30, 31, 32, 33, 34 and 35:

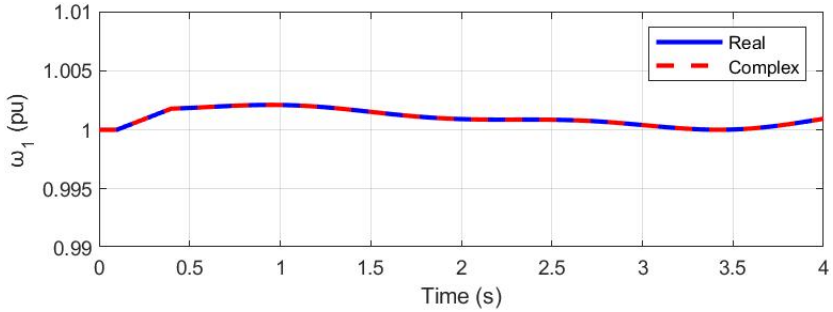

Figure 26 – ω_1 for the Machine 1 of the 39-Bus IEEE System

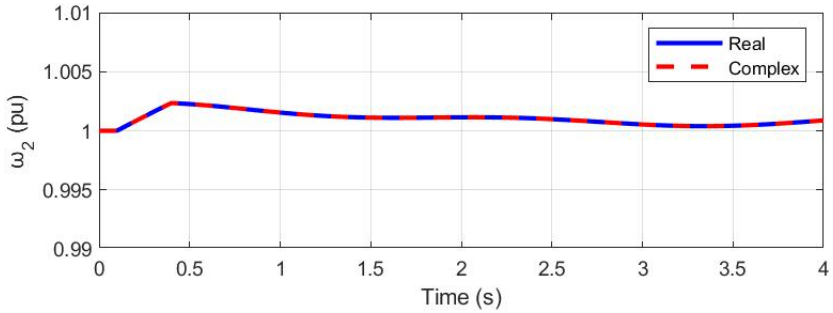

Figure 27 – ω_2 for the Machine 2 of the 39-Bus IEEE System

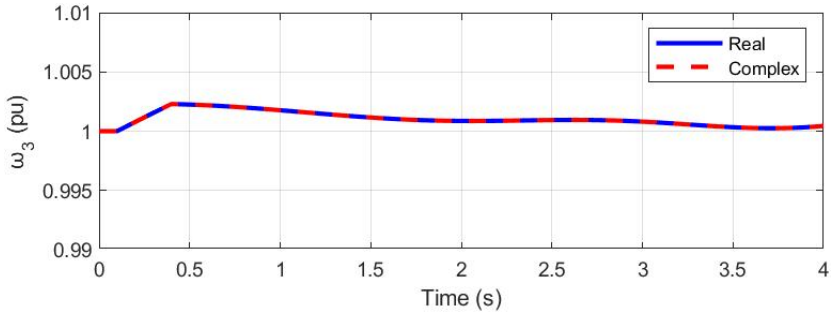

Figure 28 – ω_3 for the Machine 3 of the 39-Bus IEEE System

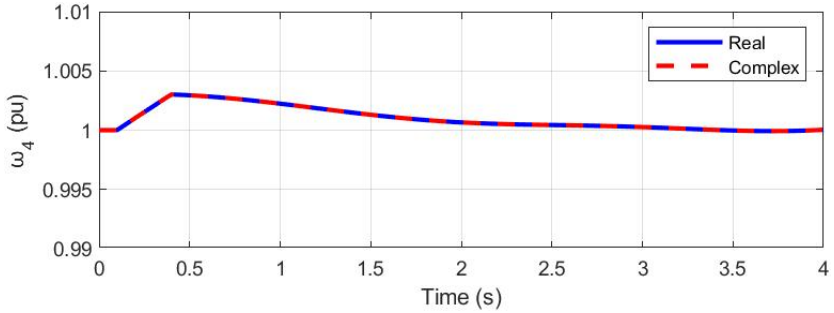

Figure 29 – ω_4 for the Machine 4 of the 39-Bus IEEE System

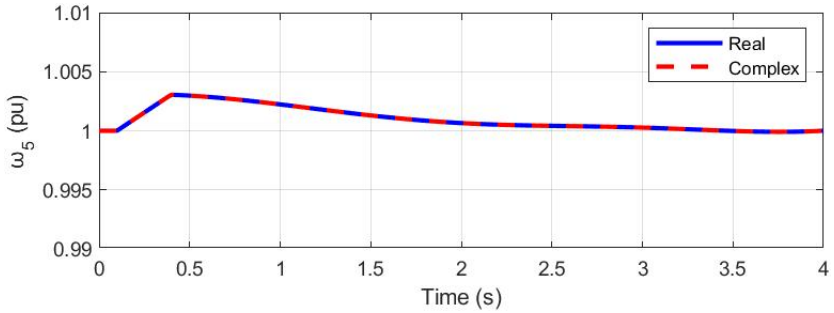

Figure 30 – ω_5 for the Machine 5 of the 39-Bus IEEE System

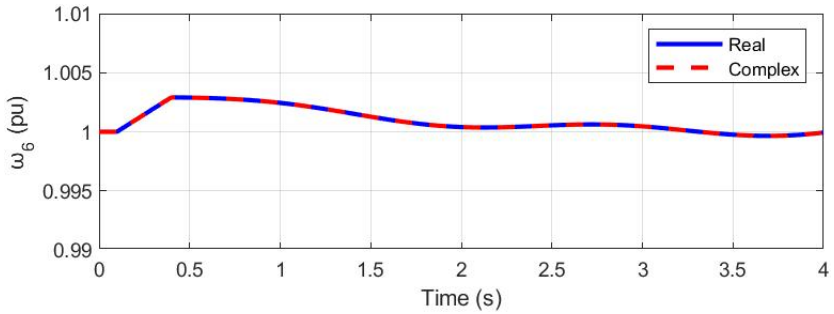

Figure 31 – ω_6 for the Machine 6 of the 39-Bus IEEE System

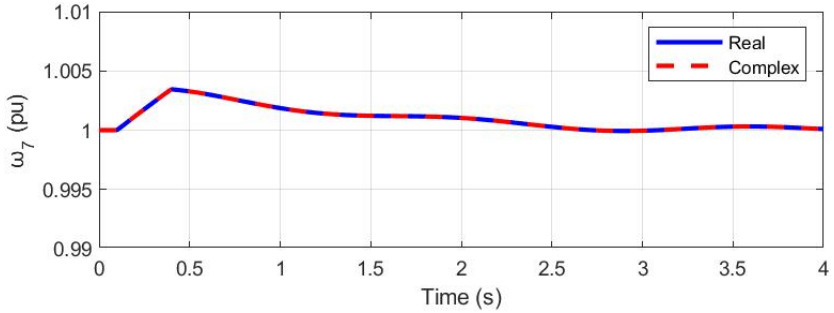

Figure 32 – ω_7 for the Machine 7 of the 39-Bus IEEE System

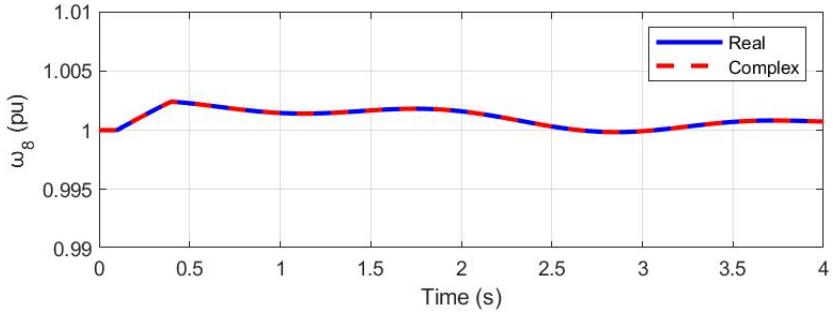

Figure 33 – ω_8 for the Machine 8 of the 39-Bus IEEE System

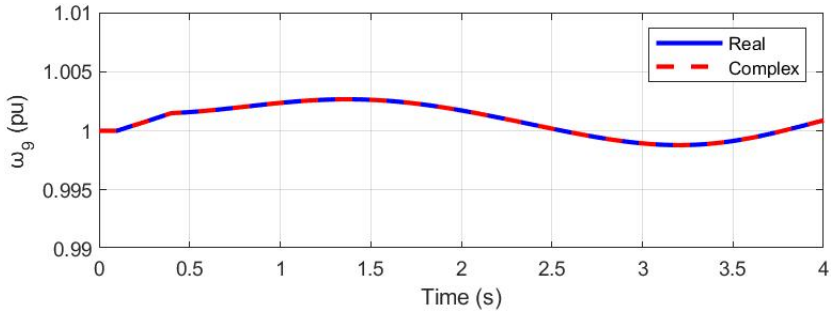

Figure 34 – ω_9 for the Machine 9 of the 39-Bus IEEE System

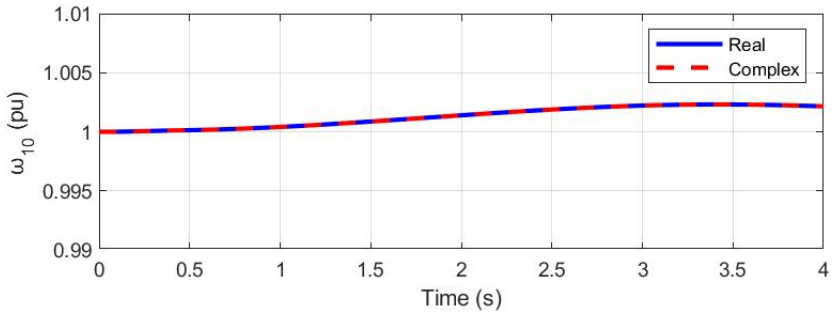

Figure 35 – ω_{10} for the Machine 10 of the 39-Bus IEEE System

Observing the previous MATLAB graphics, the complex variable ω tracks the real variable for each machine. These were expected results and it can be resumed on a comparative real graphic on Figure 36,

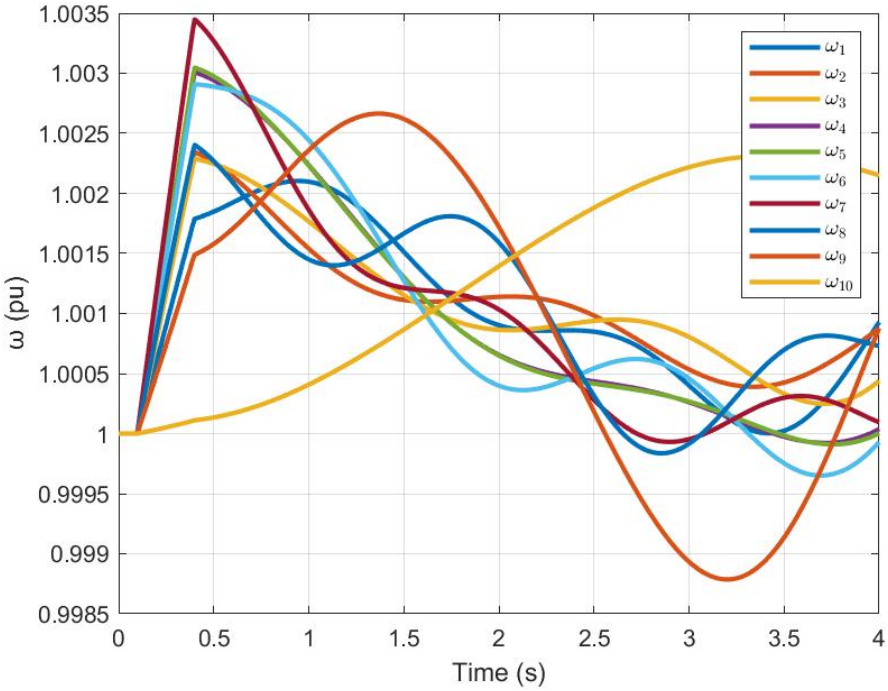

Figure 36 – Comparative for ω of Each Machine of the 39-Bus IEEE System

Then, comparing of the ω_9 obtained from SIMULINK, using all the variable steps integration methods, with ORGANON for this system:

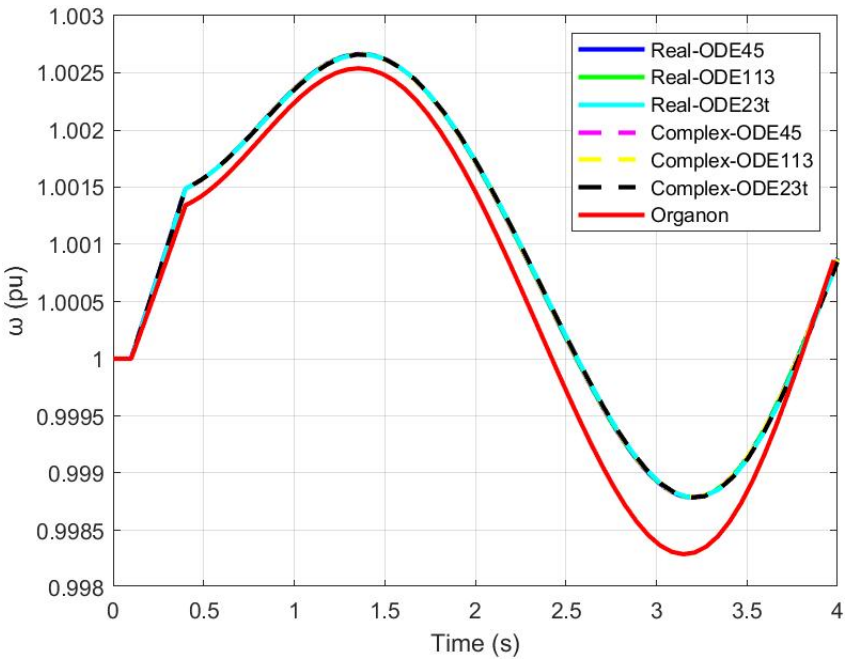

Figure 37 – ω_9 of Machine 9 on SIMULINK and on ORGANON

Looking on Figure 37, it verifies that the state variable of the ninth machine, ω_9, formulated on complex and real planes implemented, is pratically equal the dynamics with the validation program, ORGANON. For every integration method, the difference between complex and real planes is at certain instant 10^{-15} *p.u.*.

The three integration methods, with variable steps, are equally distant to ORGANON, for instance, on $3,15s$ these variable integration steps methods have $0,9988$ p.u., a difference of 0,0005 p.u. to ORGANON, as seen on Table 8.

Now, it will be presented the result for δ_{91},

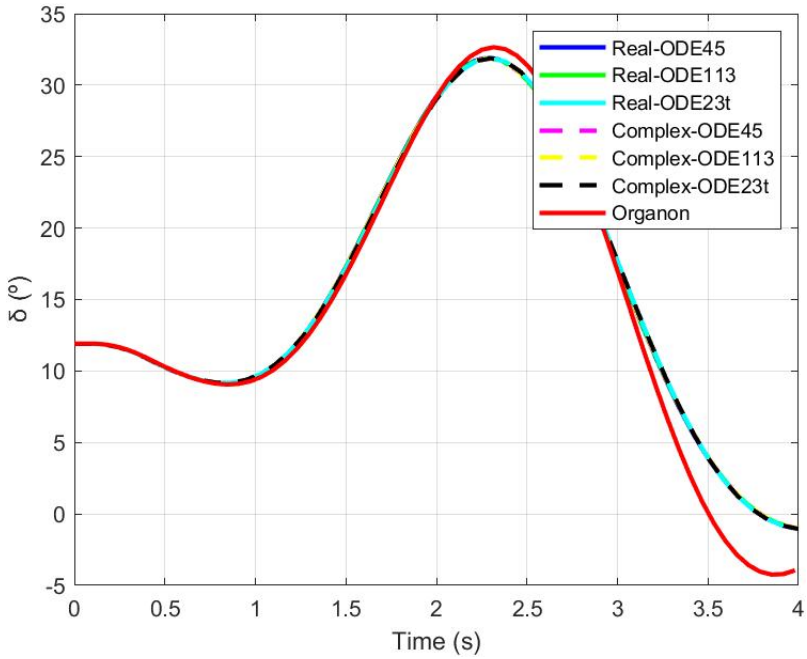

Figure 38 – δ_{91} of the 39-Bus IEEE System

As it can be seen on Figure 38, until the applying of short circuit, the angle δ_{91} keeps continuous because of its steady state. After 0,1s, the angle of the machine 9 has a not convergent comportment, holding it same after removing the fault in 0,4s. Utilizing the 3 integration methods (ODE45, ODE113 and ODE23t) from SIMULINK, both graphics in real and complex domains have the same dynamics with the graphic of ORGANON for this state variable. But, the closest integration method is the trapezoidal, for instance, on $3,90s$ this method has $-0,78°$ for δ_{91} and ORGANON results $-4,25°$ for the same state variable, a difference of $3,47°$, how observed on Table 8.

Table 8 – Values of Simulink Integration Methods and of Organon - 39-Bus IEEE

39 - Bus IEEE System							
IM	Variables				ORGANON	Variables	
	Real		Complex			Real	
	$\delta_{91}^{\circ}\ (t = 3,90s)$	$\omega_9\ (t = 3,15s)$	δ_{91}°	ω_9		δ_{91}°	ω_9
$ODE45$	$-0,73$	$0,9988$	$-0,73$	$0,9988$			
$ODE113$	$-0,70$	$0,9988$	$-0,70$	$0,9988$		$-4,25$	$0,9983$
$ODE23t$	$-0,78$	$0,9988$	$-0,78$	$0,9988$			

Looking the dynamics of δ_{91} and ω_9 when using the fix and variable integration step methods, $ODE4$, $ODE45$, $ODE23t$ and $ODE113$,respectively, the one that repre-

sents better is the fix integration step method, with the same used absolute and relative tolerances in ORGANON. These integration methods are detailed on appendix C and in D, respectively.

For the last, seeing the convergence of the IEEE 39-bus system on Figure 39,

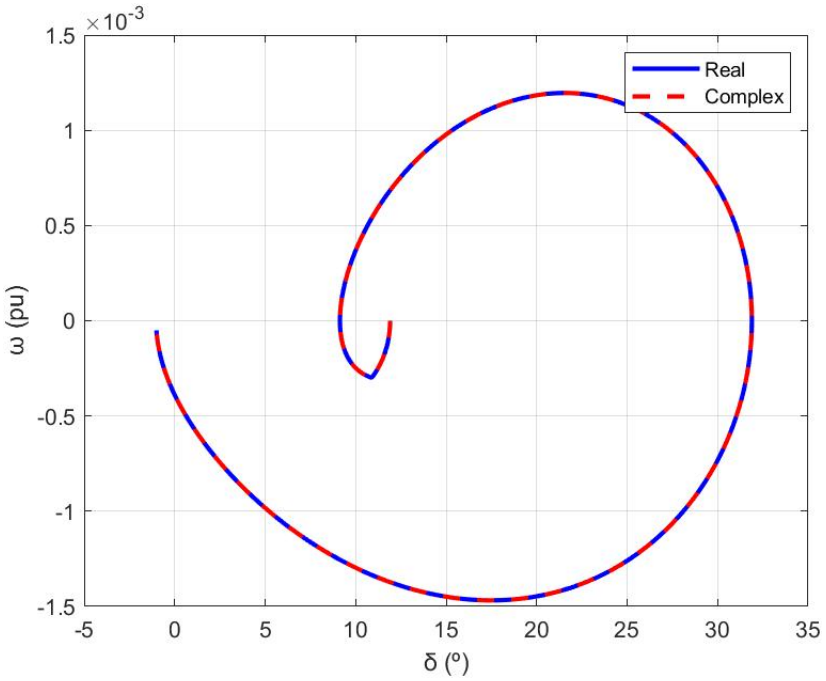

Figure 39 – Convergence of δ During the Event on the 39-Bus IEEE System

Noting that the absolute and relative tolerance for the dynamic simulation used in ORGANON for both systems is 10^{-4}. These tolerances in ORGANON affect the integrations methods results in SIMULINK.

How observed on last graphic, initially, the δ and ω have its values on steady state. After a short circuit, the both state variables change its operating points until to achieve a new diverged operational point on 4s. It can conclude that the real and complex planes formulations have the same operating dynamic. Therefore, the theory presented, on [1, 8, 27, 43, 44], matches with this second study case.

Now, comparing the results for δ and ω in real and complex planes with ORGANON using a simulation of $0.35s$,

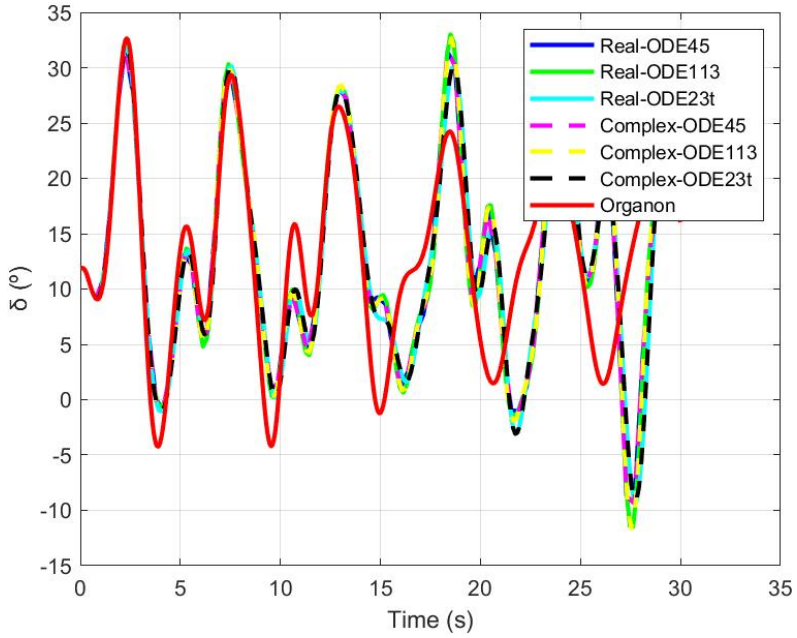

Figure 40 – δ_{91} of the 39-Bus IEEE System

It can be observed that until approximately $12s$ the δ_{91} keeps the same dynamics in real and in complex plane on SIMULINK and on ORGANON. From, this time, its dynamics start diverging with ORGANON for the three integration methods.

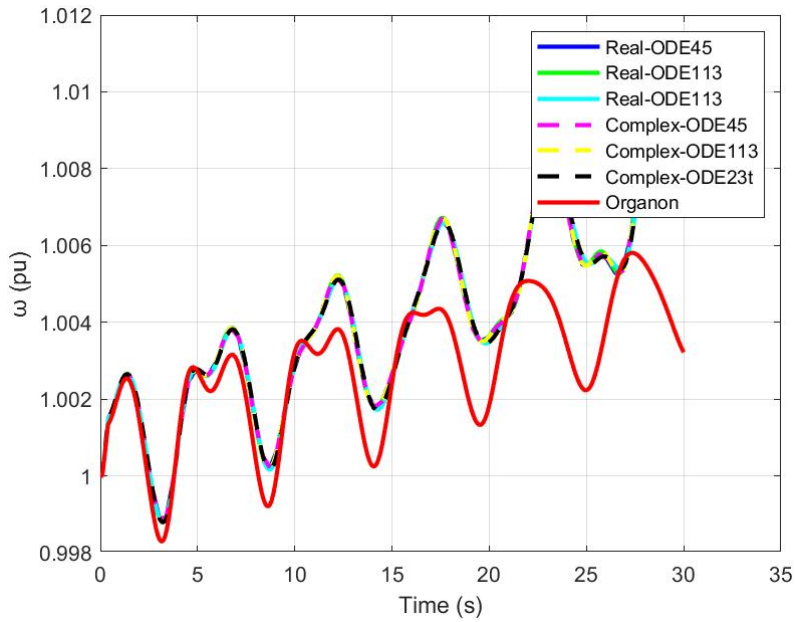

Figure 41 – ω_9 of the 39-Bus IEEE System

It can be noted from 41, that the dynamic for the three integration methods diverge from ORGANON from around $12s$.

A flowchart can summarize the process to get the dynamic simulations for real and complex planes in MATLAB and SIMULINK as seen in Figure 42,

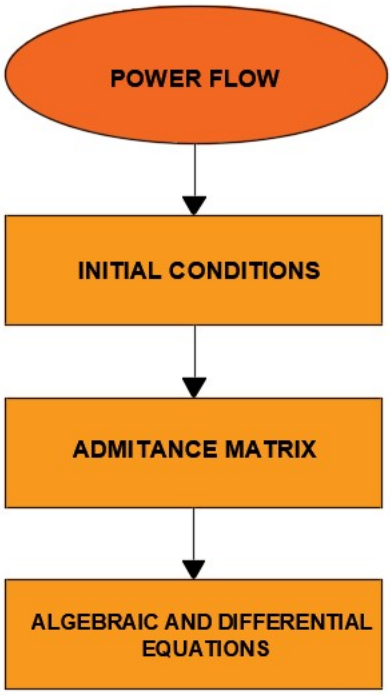

Figure 42 – Flowchart to Obtain the State Variables in Complex and Real Planes

4.3 Performance of The Dynamic Machine Model in Real and Complex Planes

In this section, it will be discussed the time simulation in real and complex planes, respectively.

4.3.1 Performance of the Classical Model

Simulating the classical models for the both systems on real and complex planes, result the table 9,

Table 9 – Simulations Times for Complex and Real Planes

System	Fault	Nearby Bus	$t_{real}\ [s]$	$t_{complex}\ [s]$	$t_{dif}\ [s]$
IEEE -9 Bus	$Line_{(8-9)}$	8	$0,2311$	$0,2095$	$0,0216$
IEEE -39 Bus	$Line_{(14-15)}$	15	$0,2643$	$0,2430$	$0,0213$

How it can see on previous table, the electric machine model on complex plane is close, but a little bit higher than real one for both systems. Proving that dealing with algorithims in complex domain are better than the one in real plane because of the processing velocity.

5 General Conclusions

The studies in complex plane was made with the MATLAB algorithm and the equations on SIMULINK. It can realize that using the IEEE 9-bus and IEEE 39-bus the processing speed is close, but a little bit higher than real one for both systems. But considering that power systems with more numbers of bus, it should pay attention how is the time characteristics because there are many involving variables.

Besides it, it can be concluded too that how many more bus in the system, less quick are the convergences using the classical machine model on complex plane.

It also showed that the real and complex domains answers got for the systems on simulations programs (SIMULINK/MATLAB and ORGANON) have the same dynamics on transient and on steady state. How it was expected. And the best and closest integration method to represent the real and complex planes is with fix step, with the same used absolute and relative tolerances in ORGANON.

It can be concluded that the SIMULINK and ORGANON have the same operating points on steady state, because its power flow solutions have the same results. And until around $12s$ the operating points keep approximately the same dynamic the real and complex planes with ORGANON. These differences are due to the absolute and relative tolerances for the dynamic simulation used in ORGANON. These tolerances in ORGANON affect the integrations methods results in SIMULINK. Therefore, new tests should be done to match the dynamics in ORGANON and SIMULINK.

The condition to the machines diverge was with clear fault on $0.5s$. It can be realized that some machines diverge from this time. I.e., from this time some machines escape its stability conditions.

Futhermore, the implementation in complex and real planes have few difference values for δ and ω for both IEEE systems. Satisfying, mathematically, the implementation in complex plane comparing its results with ORGANON.

5.1 Future Works

It is known that the global trend of the power electric systems is to make use of more efficient models for equipments. This implies on more researches in more efficient models. Knowing the machines on this work were modeled using the simplest representation, known as classical model. A machine model in complex domain more complete should be looked for to represent better the electric systems. This complex modeling is relevant to investigate. In this scenario, the researches in complex plane on power system

are extremely important. In this field, this concept has been studied for many applications, remaining, also, the formulation in complex plane of the governor and the excitation. This topic, in complex domain, is interesting to study.

Besides it, knowing that the real analysis of stability on power system has as focus the study of capacity of a determined power system to keep its synchronism when submitted to huge disturbs. A recent opportunity with this work is to investigate the comportment of stability considering the complex plane, taking into account its root methods, characteristic polynomial and other aspects [45, 46].

For last, new applications using this classical model in complex plane can be researched, such as: the power system planning, operating and monitoring; power system state estimation and others. Because of the complex linearized funtion, making possible, to use the Wirtinger Calculous [47, 48, 49, 17, 50, 51]

Bibliography

1 MELLO, F. de; ELETROBRÁS.; MARIA, F. U. of S. *Dynamics of Electric Machines*. [S.l.]: Federal University of Santa Maria, 1979. (Course of Electric Power Systems Engineering - PTI Series). 10, 17, 19, 20, 21, 22, 25, 28, 29, 30, 36, 50, 59

2 CHAPMAN, S. *Electric Machines*. [S.l.]: McGraw-Hill Interamericana de España S.L., 2005. ISBN 9789701049471. 10, 20, 31, 37

3 MOURA, A.; MOURA, A.; ROCHA, E. *Analysis of Power Flow in Power System*. [S.l.: s.n.], 2018. ISBN 978-85-88098-83-1. 10, 45

4 ATHAY, T.; PODMORE, R.; VIRMANI, S. A practical method for the direct analysis of transient stability. *IEEE Transactions on Power Apparatus and Systems*, PAS-98, n. 2, p. 573–584, 1979. 10, 51

5 FUCHS, R. *Electric Power Transmission*. [S.l.]: Scientific and Technic Books, 2015. 17

6 STEIN, R. *Electric Power System Components: Transformers and Rotating Machines*. [S.l.]: Springer Netherlands, 2013. ISBN 9789401713948. 17

7 KNIGHT, U. *Power Systems in Emergencies: From Contingency Planning to Crisis Management*. [S.l.]: Wiley, 2001. ISBN 9780471490166. 17

8 KUNDUR, P. *Power System Stability and Control*. [S.l.]: McGraw-Hill Education, 1993. 17, 36, 38, 50, 59

9 FURINI, M. A.; ARAUJO, P. B. Improvements of the dinamic stability of power system of multimachines using facts devices tcsc. In: *Control and Automation*. [S.l.: s.n.], 2008. v. 19, n. 2, p. 214–225. 17

10 KIMPARA, M. L. M. *Modeling and Analysis of Syncronous Generator using the Field Reconstruction Method*. 2012. 17

11 BILA, C. *Power System Dynamic State Estimation and Load Modeling*. Tese (Doutorado) — Northestern University, 2013. 17

12 ANDERSON, P. M. *Power System Control and Stability*. [S.l.]: Science Press, 1977. 17, 38, 44, 69

13 ADIBI, M.; HIRSCH, P.; JORDAN, J. Solution methods for transient and dynamic stability. *Proceedings of the IEEE*, v. 62, n. 7, p. 951–958, 1974. 17, 36

14 ARRILLAGA, J.; ARNOLD, C. *Computer Analysis of Power Systems*. [S.l.]: Wiley, 1990. ISBN 9780471927600. 17

15 CHEN, H. et al. Dynamic simulation of electric machines on fpga boards. In: *2009 IEEE International Electric Machines and Drives Conference*. [S.l.: s.n.], 2009. p. 1523–1528. 17

16 RUGGIERO, M.; LOPES, V. da R. *Numeric Calculous: Computational and Theoric Aspects*. Pearson Universities, 2000. ISBN 9788534602044. Disponível em: <https://books.google.com.br/books?id=kuRDAAAACAAJ>. 17, 45, 51, 73, 74, 76

17 PIRES, R. C.; MILI, L.; LEMOS, F. A. B. Constrained Robust Estimation of Power System State Variables and Transformer Tap Positions Under Erroneous Zero-Injections. *IEEE Transactions on Power Systems*, IEEE, v. 29, p. 1144–1152, 2014. ISSN 0885-8950,1558-0679. Disponível em: <http://doi.org/10.1109/TPWRS.2013.2284734>. 17, 63

18 PIRES, R.; MILI, L.; CHAGAS, G. Robust complex-valued Levenberg-Marquardt algorithm as applied to power flow analysis. *International Journal of Electrical Power and Energy Systems*, Elsevier, v. 113, n. May, p. 383–392, 2019. ISSN 01420615. Disponível em: <https://doi.org/10.1016/j.ijepes.2019.05.032>. 17

19 MALDONADO, M. A. R. *Developing the Mathematical Models Representing the Dynamic Comportament of Microturbines to the Conection in Electric Power System*. Tese (Doutorado) — Federal University of Itajuba, 2010. 18

20 GLOVER, J.; OVERBYE, T.; SARMA, M. *Power System Analysis and Design*. [S.l.]: Cengage Learning, 2016. ISBN 9781305886957. 18, 36

21 NISE, N. *Engenharia De Sistemas De Controle*. LTC, 2012. ISBN 9788521621355. Disponível em: <https://books.google.com.br/books?id=ZsXINAEACAAJ>. 18

22 CHIASSON, J. *Modeling and High Performance Control of Electric Machines*. [S.l.]: Wiley, 2005. (IEEE Press). ISBN 9780471722342. 20

23 FITZGERALD, A.; KINGSLEY, C.; UMANS, S. *Power Electric Machines 6th*. [S.l.]: Bookman, 2006. ISBN 9788560031047. 21, 28

24 ZANETTA, L. *Fundamentals of Power Electric Systems*. Editora Livraria da Física, 2006. ISBN 9788588325418. Disponível em: <https://books.google.com.br/books?id=Nyep7l_kBFkC>. 22

25 DUARTE ANDERSON DE SOUSA; MOURA, A. A. F. d. Dynamic simulations comparison of syncronous machines between the anatem - cepel and the two axis model. v. 2, n. 1, p. 188–200, 2020. 24

26 MACHOWSKI, J.; BIALEK, J.; BUMBY, J. *Power System Dynamics: Stability and Control*. [S.l.]: Wiley, 2011. ISBN 9781119965053. 26, 28

27 PADIYAR, K. *Power System Dynamics: Stability and Control*. [S.l.]: Wiley, 1999. ISBN 9780471190028. 28, 50, 59

28 NAZARENO, I. S. *Mechanism of instability due to huge disturb in power electric systems modeled by algebraic differential equations*. Tese (Doutorado) — University of São Paulo State, 2009. 30

29 ZHAO, J.; NETTO, M.; MILI, L. A robust iterated extended kalman filter for power system dynamic state estimation. *IEEE Transactions on Power Systems*, v. 32, n. 4, p. 3205–3216, 2017. 36

30 TEBIANIAN, H.; JEYASURYA, B. Dynamic state estimation in power systems using kalman filters. In: *2013 IEEE Electrical Power and Energy Conference*. [S.l.: s.n.], 2013. p. 1–5. 36

31 DANDENO, P. Current usage and suggested practices in power system stability simulations for synchronous machines. *IEEE Transactions on Energy Conversion*, EC-1, n. 1, p. 77–93, 1986. 37

32 BOYCE, W.; DIPRIMA, R.; MEADE, D. *Elementary Differential Equations*. LTC, 2020. ISBN 9788521636946. Disponível em: <https://books.google.com.br/books?id=DRr8zwEACAAJ>. 38

33 FERREIRA, C. *Linear Newtowkrs in Power Electric Systems*. [S.l.]: Canal Energia, 2005. ISBN 9788598052038. 42

34 LOAD representation for dynamic performance analysis (of power systems). *IEEE Transactions on Power Systems*, v. 8, n. 2, p. 472–482, 1993. 42

35 CALISKAN, S. Y.; TABUADA, P. Towards kron reduction of generalized electrical networks. *Automatica*, v. 50, n. 10, p. 2586–2590, 2014. ISSN 0005-1098. Disponível em: <https://www.sciencedirect.com/science/article/pii/S0005109814003331>. 43

36 HOSSAIN, E. *MATLAB and Simulink Crash Course for Engineers*. [S.l.]: Springer International Publishing, 2022. ISBN 9783030897628. 44, 74, 75

37 VIEIRA, C.; MORAIS, W. *Matlab - Complete Course*. [S.l.]: FCA, 2013. ISBN 9789727227051. 44, 75, 76

38 CHAVES, S. *Static and Dynamic Analysis of Power System Through Integrated Computational Program: ORGANON*. 2008. 44

39 SILVA, L. et al. *Tutorial of ANAREDE Program with Power Electric System Settings*. [S.l.: s.n.], 2017. ISBN 9781521367094. 44

40 MOURA A.P DE; ROCHA, E. *Exercises of Power Flow*. [S.l.]: Artliber, 2018. ISBN 9788588098848. 44

41 MONTICELLI, A.; (BRAZIL), R. C. of E. E. *Power Flow in Electric Power System*. [S.l.]: E. Blucher, 1983. 45, 51

42 USER'S Guide of Mathpower 8.01b. [S.l.], 2024. 45, 51

43 TAYLOR, C.; BALU, N.; MARATUKULAM, D. *Power System Voltage Stability*. [S.l.]: McGraw-Hill, 1994. (EPRI power system engineering series). ISBN 9780070631847. 50, 59

44 RAMOS, D.; DIAS, E. *Electric Power Systens: Steady State*. [S.l.]: Guanabara Dois, 1982. 50, 59

45 SOUZA, A. de; PINHEIRO, C. *Introduction to Modelling Analysis and Simulation of Dynamic Systems*. Interciciencia, 2008. ISBN 9788571931886. Disponível em: <https://books.google.com.br/books?id=00w8QwAACAAJ>. 63

46 OGATA, K. *Engineering of Modern Control*. Pearson Universities, 2010. ISBN 9788576058106. Disponível em: <https://books.google.com.br/books?id=iL3FYgEACAAJ>. 63

47 WIRTINGER, W. Zur formalen Theorie der Funktionen von mehr komplexen Veranderlichen. *Mathematische Annalen*, v. 97, n. 1, p. 357–375, dec 1927. ISSN 0025-5831. Disponível em: <http://link.springer.com/10.1007/BF01447872>. 63

48 RESENDE, E. M. *Robust State Estimation Based on Remote Monitoring via PMU and SCADA - Unified Solution in the Complex Plan*. Dissertação (Mestrado) — UNIFEI, 2022. Disponível em: <https://repositorio.unifei.edu.br/jspui/handle/123456789/2934>. 63

49 DZAFIC, I.; JABR, R. A.; HRNJIC, T. Hybrid State Estimation in Complex Variables. *IEEE Transactions on Power Systems*, v. 33, n. 5, p. 5288–5296, 2018. ISSN 08858950. 63

50 MILI, L. et al. Robust state estimation based on projection statistics [of power systems]. *IEEE Transactions on Power Systems*, IEEE, v. 11, p. 1118–1127, 1996. ISSN 0885-8950,1558-0679. Disponível em: <http://doi.org/10.1109/59.496203>. 63

51 ZHAO, J. et al. Roles of dynamic state estimation in power system modeling, monitoring and operation. *IEEE Transactions on Power Systems*, v. 36, n. 3, p. 2462–2472, 2021. 63

52 ZSMJ. *Power System Data*. 2024. Available at: <https://sites.google.com/site/powersystemdata>. Accessed in: May, 15th. 69, 70

Appendix

APPENDIX A – 9-Bus System Data

This 9-bus system was defined in [12] and its data are shown on tables 10, 11 and 12, respectively. However, this data also can be accessed in [52].

Table 10 – Line Data for IEEE - 9 Bus System

Element	$R\,[p.u.]$	$X\,[p.u.]$	$B\,[MVar]$	$S_b\,[MVA]$
$Line_{(2-7)}$	–	0,0576	–	100
$Line_{(7-8)}$	0,0085	0,072	14,90	100
$Line_{(5-7)}$	0,032	0,161	30,60	100
$Line_{(8-9)}$	0,0119	0,1008	20,90	100
$Line_{(4-5)}$	0,01	0,085	17,60	100
$Line_{(3-9)}$	–	0,0576	–	100
$Line_{(6-9)}$	0,039	0,17	35,80	100
$Line_{(4-6)}$	0,017	0,092	15,80	100
$Line_{(1-4)}$	–	0,0576	–	100

Table 11 – Machine Data for IEEE - 9 Bus System

Element	R_a [p.u]	X'_d [p.u]	H [MJ/MVA]	D_m[p.u]	S_b[MVA]
$Generator-1$	0,0	0,06080	23,64	0,0255	1000
$Generator-2$	0,0	0,11980	6,4	0,00663	800
$Generator-3$	0,0	0,18130	3,01	0,00265	800

Table 12 – Operative Conditions for IEEE - 9 Bus System

Element	Bus ♯	P_G [MW]	V_t [p.u]	P_L [MW]	Q_L [MVar]
$Generator(1)$	1	–	1,04	–	–
$Generator(2)$	2	163	1,025	–	–
$Generator(3)$	3	85	1,025	–	–
$Load\,(A)$	5	–	–	125	50
$Load\,(B)$	6	–	–	90	30
$Load\,(C)$	8	–	–	100	35

APPENDIX B – IEEE 39-Bus System Data

This IEEE 39-bus system is known as *New England Test System* and its data are shown on tables 13, 14 and 15, respectively. However, this data also can be accessed in [52].

Table 13 – Line Data for IEEE - 39 Bus System

Element	$R\,[p.u.]$	$X\,[p.u.]$	$B\,[MVar]$	$S_b\,[MVA]$
$Line_{(2-30)}$	$0,0000$	$0,0181$	0	100
$Line_{(1-2)}$	$0,0035$	$0,0411$	$69,87$	100
$Line_{(1-39)}$	$0,0010$	$0,0250$	75	100
$Line_{(9-39)}$	$0,0010$	$0,0250$	120	100
$Line_{(8-9)}$	$0,0023$	$0,0363$	$38,04$	100
$Line_{(25-37)}$	$0,0006$	$0,0232$	0	100
$Line_{(2-25)}$	$0,0070$	$0,0086$	$14,60$	100
$Line_{(2-3)}$	$0,0013$	$0,0151$	$25,72$	100
$Line_{(3-4)}$	$0,0013$	$0,0213$	$22,14$	100
$Line_{(4-5)}$	$0,0008$	$0,0128$	$13,42$	100
$Line_{(5-8)}$	$0,0008$	$0,0112$	$14,76$	100
$Line_{(5-6)}$	$0,0002$	$0,0026$	$4,34$	100
$Line_{(6-7)}$	$0,0006$	$0,0092$	$11,30$	100
$Line_{(7-8)}$	$0,0004$	$0,0046$	$7,80$	100
$Line_{(25-26)}$	$0,0032$	$0,0323$	$51,30$	100
$Line_{(3-18)}$	$0,0011$	$0,0133$	$21,38$	100
$Line_{(4-14)}$	$0,0008$	$0,0129$	$13,82$	100
$Line_{(6-11)}$	$0,0007$	$0,0082$	$13,89$	100
$Line_{(6-31)}$	$0,0000$	$0,0250$	0	100
$Line_{(17-18)}$	$0,0007$	$0,0082$	$13,19$	100
$Line_{(15-16)}$	$0,0009$	$0,0094$	$17,10$	100
$Line_{(14-15)}$	$0,0018$	$0,0217$	$36,60$	100
$Line_{(13-14)}$	$0,0009$	$0,0101$	$17,23$	100
$Line_{(12-13)}$	$0,0016$	$0,0435$	0	100
$Line_{(11-12)}$	$0,0016$	$0,0435$	0	100
$Line_{(10-11)}$	$0,0004$	$0,0043$	$7,29$	100
$Line_{(10-13)}$	$0,0004$	$0,0043$	$7,29$	100

Continued on next page

Table 13 – *Continuation of table*

Element	$R\,[p.u.]$	$X\,[p.u.]$	$B\,[MVar]$	$S_b\,[MVA]$
$Line_{(10-32)}$	$0,0000$	$0,0200$	0	100
$Line_{(26-29)}$	$0,0057$	$0,0625$	$102,9$	100
$Line_{(26-28)}$	$0,0043$	$0,0474$	$78,02$	100
$Line_{(26-27)}$	$0,0014$	$0,0147$	$23,96$	100
$Line_{(17-27)}$	$0,0013$	$0,0173$	$32,16$	100
$Line_{(16-17)}$	$0,0007$	$0,0089$	$13,42$	100
$Line_{(16-19)}$	$0,0016$	$0,0195$	$30,40$	100
$Line_{(19-20)}$	$0,0007$	$0,0138$	0	100
$Line_{(20-34)}$	$0,0009$	$0,0180$	0	100
$Line_{(28-29)}$	$0,0014$	$0,0151$	$24,90$	100
$Line_{(29-38)}$	$0,0008$	$0,0156$	0	100
$Line_{(16-21)}$	$0,0008$	$0,0135$	$25,48$	100
$Line_{(16-24)}$	$0,0003$	$0,0059$	$6,80$	100
$Line_{(23-24)}$	$0,0022$	$0,0350$	$36,10$	100
$Line_{(19-33)}$	$0,0007$	$0,0142$	0	100
$Line_{(23-36)}$	$0,0005$	$0,0270$	0	100
$Line_{(21-22)}$	$0,0008$	$0,0140$	$25,65$	100
$Line_{(22-23)}$	$0,0006$	$0,0096$	$18,46$	100
$Line_{(22-35)}$	$0,0000$	$0,0143$	0	100

End of table

Table 14 – Machine Data for IEEE - 39 Bus System

Element	R_a [p.u]	X'_d [p.u]	H [MJ/MVA]	D_m[p.u]	S_b[MVA]
$Generator-1$	0	$0,3$	42	$0,05$	300
$Generator-2$	0	$0,3$	$30,3$	$0,05$	600
$Generator-3$	0	$0,3$	$35,8$	$0,05$	700
$Generator-4$	0	$0,3$	$28,6$	$0,05$	700
$Generator-5$	0	$0,3$	26	$0,05$	550
$Generator-6$	0	$0,3$	$34,8$	$0,05$	700
$Generator-7$	0	$0,3$	$26,4$	$0,05$	600
$Generator-8$	0	$0,3$	$24,3$	$0,05$	600
$Generator-9$	0	$0,3$	$34,5$	$0,05$	1000
$Generator-10$	0	$0,3$	500	$0,05$	1000

Table 15 – Operative Conditions for IEEE - 39 Bus System

Element	Bus ♯	P_G [MW]	V_t [p.u]	P_L [MW]	Q_L [MVar]
$Generator(1)$	30	250	$1,027$	–	–
$Generator(2)$	31	–	$0,982$	$9,2$	$4,6$
$Generator(3)$	32	650	$0,983$	–	–
$Generator(4)$	33	632	$0,997$	–	–
$Generator(5)$	34	508	$1,012$	–	–
$Generator(6)$	35	560	$1,033$	–	–
$Generator(7)$	36	650	$1,029$	–	–
$Generator(8)$	37	540	$1,027$	–	–
$Generator(9)$	38	830	$1,026$	–	–
$Generator(10)$	39	1000	$1,020$	1104	250
$Load\,(1)$	25	–	–	224	$47,2$
$Load\,(2)$	27	–	–	281	$75,5$
$Load\,(3)$	39	–	–	1104	250
$Load\,(4)$	28	–	–	206	$27,6$
$Load\,(5)$	29	–	–	$283,5$	$26,9$
$Load\,(6)$	26	–	–	139	17
$Load\,(7)$	3	–	–	322	$2,4$
$Load\,(8)$	18	–	–	158	30
$Load\,(9)$	16	–	–	$329,4$	$32,3$
$Load\,(10)$	21	–	–	274	115
$Load\,(11)$	4	–	–	500	184
$Load\,(12)$	24	–	–	$308,6$	-92
$Load\,(13)$	23	–	–	$247,5$	$84,6$
$Load\,(14)$	12	–	–	$7,5$	88
$Load\,(15)$	7	–	–	$233,8$	84
$Load\,(16)$	8	–	–	522	176
$Load\,(17)$	31	–	–	$9,2$	$4,6$
$Load\,(18)$	20	–	–	628	103
$Load\,(19)$	15	–	–	320	153

APPENDIX C – Integration Methods with Fixed Step

D.1 **Runge-Kutta (ODE4)**

In numerical analysis, the Runge–Kutta methods were developed around 1900 by the German mathematicians Carl Runge and Wilhelm Kutta. And the most used RK method is the fourth order method and it has the expression (C.1) [16],

$$y_i = y_{i-1} + \frac{1}{6}\ [k_1 + 2\ k_2 + 2\ k_3 + k_4]\,, \tag{C.1}$$

where,

$$k_1 = h\ f(x_{i-1}, y_{i-1}) \tag{C.2}$$

$$k_2 = h\ f(x_{i-1} + h/2, y_{i-1} + k_1/2) \tag{C.3}$$

$$k_3 = h\ f(x_{i-1} + h/2, y_{i-1} + k_2/2) \tag{C.4}$$

$$k_4 = h\ f(x_{i-1} + h, y_{i-1} + k_3) \tag{C.5}$$

For $i = 1, 2, ..., n$ iterations.

APPENDIX D – Integration Methods with Variable Step

C.1 **Dormand-Prince (ODE45)**

In numerical analysis, the Dormand–Prince method, is a method for solving ordinary differential equations (ODE). The method is a member of the Runge–Kutta family of ODE solvers. More specifically, it uses six function evaluations to calculate the fourth and fifth order solutions. The difference between these solutions is then taken to be the error of the fourth-order solution. This error estimate is very convenient for adaptive stepsize integration algorithms [16, 36].

$$x_{k+1} = x_k + h \sum_{i=1}^{m} \gamma_i \; k_i, \tag{D.1}$$

where,

$$k_i = f \left(t_k + a_i \; h, x_k + h \sum_{j=1}^{i-1} \beta_j \; k_j \right), \tag{D.2}$$

beeing $i = 1, 2, 3..., m$.

Also, the coeficients of β_j, a_i and γ_i are given by Butcher matrix on first, second and third quadrant, respectively,

0							
1/5	1/5						
3/10	3/40	9/40					
4/5	44/45	−56/15	32/9				
8/9	19372/6561	−25360/2187	64448/6561	−212/729			
1	9017/3168	−355/33	46732/5247	49/176	−5103/18656		
1	35/384	0	500/1113	125/192	−2187/6784	11/84	
	5179/57600	0	7571/16695	393/640	−92097/339200	187/2100	1/40
	35/384	0	500/1113	125/192	−2187/6784	11/84	0

Table 16 – Blutcher Matrix for Dormand-Prince Coefficients

Therefore, the Dormand–Prince method has seven stages, but it uses only six function evaluations per step because it has the "First Same As Last" property: the last stage is evaluated at the same point as the first stage of the next step. Dormand and Prince chose the coefficients of their method to minimize the error of the fifth-order solution. This method is more suitable when the higher-order solution is used to continue the integration, a practice known as local extrapolation.

Dormand–Prince is the default method in the ODE45 solver for MATLAB and is the default choice for the SIMULINK solver [36, 37].

*C.*2 **Trapezoidal (ODE23t)**

This method allows to calculate the approximate integral of $f(x)$, i.e., ODE function, through the sums of trapezium areas defined by the representation of points of an ODE in a cartesian plane. The Figure 43 shows this idea,

x	$a = x_0$	x_1	x_2	$b = x_3$
$f(x)$	$f(x_0)$	$f(x_1)$	$f(x_2)$	$f(x_3)$

Table 17 – Points of f(x)

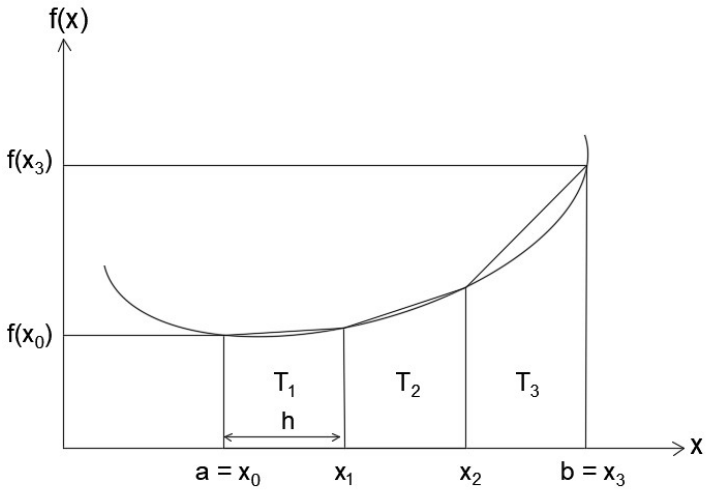

Figure 43 – Function f(x)

Note that,

$$T_1 = \frac{f(x_0) + f(x_1)}{2}\, h, \tag{D.3}$$

$$T_2 = \frac{f(x_1) + f(x_2)}{2}\, h, \tag{D.4}$$

$$T_3 = \frac{f(x_2) + f(x_3)}{2}\, h. \tag{D.5}$$

Thus, if 3 trapezoids are used, it results the following approximation:

$$I = \int_a^b f(x)\,dx \approx T = T_1 + T_2 + T_3, \tag{D.6}$$

Generalizing for n trapezoids,

$$T = \left[f(x_0) + 2 \sum_{i=1}^{n-1} f(x_i) + f(x_n) \right] \frac{h}{2}. \tag{D.7}$$

Observing that SIMULINK uses this method with an applied modification.

*C.*3 **Adams (ODE113)**

The Adams's method for the numerical solution of ODE is also known as the linear multistep method. Conceptually, a numerical method starts from an initial point and then takes a short step forward in time to find the next solution point. The process continues with subsequent steps to map out the solution. Knowing that multistep methods attempt to gain efficiency by keeping and using the information from previous steps rather than discarding it. Besides it, this method makes a linear combination of the previous points and uses derivative values [16, 37].

Thus, the initial values are,

$$y' = f(t, y), \tag{D.8}$$

$$y(t_0) = y_0. \tag{D.9}$$

The results are approximations for the value of $y(t)$ at discrete times t_i:

$$y_i \approx y_{t_i}, \tag{D.10}$$

Where,

$$t_i = t_0 + i\ h. \tag{D.11}$$

Where h is the time step, but sometimes referred to as Δt and i is an integer.

This multistep method use information from the previous s steps to calculate the next value. In particular, the linear multistep method uses a linear combination of y_i and

$f(t_i, y_i)$ to calculate the value of y for the desired current step. Thus, the linear multistep method is of the form:

$$\sum_{j=0}^{s} a_j \; y_{n+j} = h \; \sum_{j=0}^{s} \beta_j \; f(t_{n+j}, y_{n+j}). \tag{D.12}$$

Where a_i and β_j are the method coeficients. The coeficients should be chosen by the designer, balancing the need to get a good approximation to the true solution. Often, many coeficients are equal to zero to simplify the method.

APPENDIX E – Kron Reduction Matrix

The Kron reduction matrix, was named by the american electrical engineer, Gabriel Kron. And it is a method used to reduce or eliminate the desired node without need of repeating the steps like in Gaussian elimination.

The equation for Kron reduction is (E.1),

$$\overline{Y}_{GG}^{red} = Y_{GG} - Y_{GP}.Y_{PP}^{-1}.Y_{PG} \tag{E.1}$$

Where P and G is the number of system bus and the number of power generator, respectively;

Considering the system admittance matrix,

$$\overline{Y} = \begin{bmatrix} a_{11} & a_{12} & \dots \\ \vdots & \ddots & \\ a_{P1} & & a_{PP} \end{bmatrix} \tag{E.2}$$

The objective of the Kron reduction is becoming any system admittance matrix, a GxG matrix,

$$\overline{Y}^{red} = \begin{bmatrix} a_{11} & a_{12} & \dots \\ \vdots & \ddots & \\ a_{G1} & & a_{GG} \end{bmatrix} \tag{E.3}$$

Observing that there are three reduced matrices in dynamic systems. One before fault, $\overline{Y}_{bf}^{red}$. The second one, during fault, $\overline{Y}_{df}^{red}$. For last, the one after fault, $\overline{Y}_{af}^{red}$. The admittance matrix during fault is the same as the one before fault, however, it has the elements of the fault bus eliminated. And the admittance matrix after fault is the same as the one before fault, but its elements of the eliminated line are removed.